Article

Cell

Gut Microbiota Regulate Motor Deficits and Neuroinflammation in a Model of Parkinson's Disease

Graphical Abstract

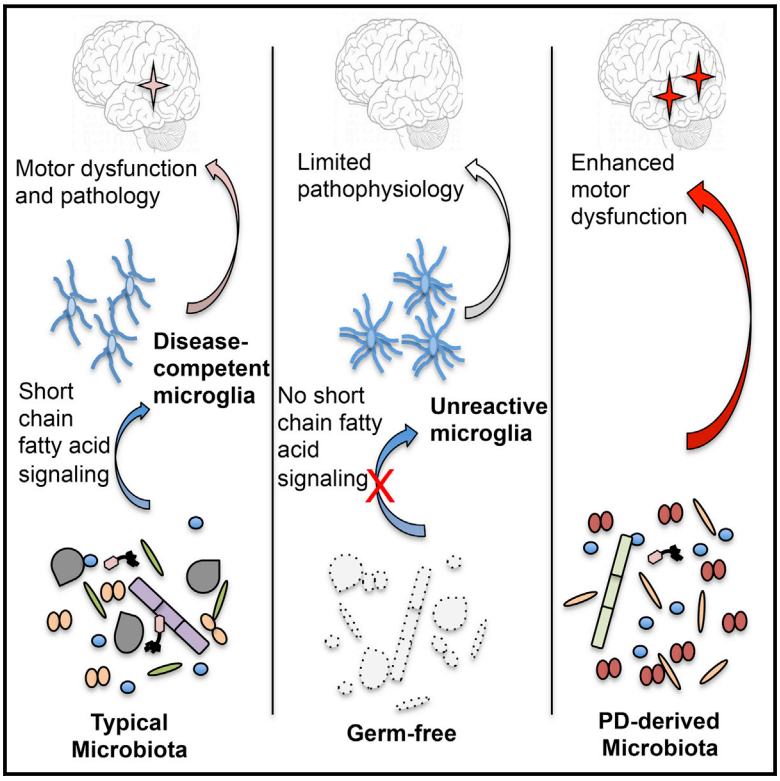

Highlights

- Gut microbes promote α-synuclein-mediated motor deficits and brain pathology
- Depletion of gut bacteria reduces microglia activation
- SCFAs modulate microglia and enhance PD pathophysiology
- Human gut microbiota from PD patients induce enhanced motor dysfunction in mice

Authors

Timothy R. Sampson, Justine W. Debelius, Taren Thron, ..., Pernilla Wittung-Stafshede, Rob Knight, Sarkis K. Mazmanian

Correspondence

trsamps@caltech.edu (T.R.S.), sarkis@caltech.edu (S.K.M.)

In Brief

Signals from gut microbes are required for the neuroinflammatory responses as well as hallmark gastrointestinal and α-synuclein-dependent motor deficits in a model of Parkinson's disease.

Sampson et al., 2016, Cell *167*, 1469–1480
December 1, 2016
http://dx.doi.org/10.1016/j.cell.2016.11.018

CellPress

Article

Cell

Gut Microbiota Regulate Motor Deficits and Neuroinflammation in a Model of Parkinson's Disease

Timothy R. Sampson,[1,*] Justine W. Debelius,[2] Taren Thron,[1] Stefan Janssen,[2] Gauri G. Shastri,[1] Zehra Esra Ilhan,[3] Collin Challis,[1] Catherine E. Schretter,[1] Sandra Rocha,[4] Viviana Gradinaru,[1] Marie-Francoise Chesselet,[5] Ali Keshavarzian,[6] Kathleen M. Shannon,[7,9] Rosa Krajmalnik-Brown,[3] Pernilla Wittung-Stafshede,[4] Rob Knight,[2,8] and Sarkis K. Mazmanian[1,10,*]

[1]Division of Biology & Biological Engineering, California Institute of Technology, Pasadena, CA 91125, USA
[2]Department of Pediatrics, University of California, San Diego, San Diego, CA 92110, USA
[3]Swette Center for Environmental Biotechnology, Biodesign Institute, Arizona State University, Tempe, AZ 85287, USA
[4]Biology and Biological Engineering Department, Chalmers University of Technology, Gothenburg 41296, Sweden
[5]Department of Neurology, The David Geffen School of Medicine at UCLA, Los Angeles, CA 90095, USA
[6]Department of Internal Medicine, Division of Gastroenterology, Rush University Medical Center, Chicago, IL 60612, USA
[7]Department of Neurological Sciences, Section of Movement Disorders, Rush University Medical Center, Chicago, IL 60612, USA
[8]Department of Computer Science and Engineering, University of California, San Diego, San Diego, CA 92093, USA
[9]Present address: Department of Neurology, University of Wisconsin-Madison, Madison, WI 53705, USA
[10]Lead Contact
*Correspondence: trsamps@caltech.edu (T.R.S.), sarkis@caltech.edu (S.K.M.)
http://dx.doi.org/10.1016/j.cell.2016.11.018

SUMMARY

The intestinal microbiota influence neurodevelopment, modulate behavior, and contribute to neurological disorders. However, a functional link between gut bacteria and neurodegenerative diseases remains unexplored. Synucleinopathies are characterized by aggregation of the protein α-synuclein (αSyn), often resulting in motor dysfunction as exemplified by Parkinson's disease (PD). Using mice that overexpress αSyn, we report herein that gut microbiota are required for motor deficits, microglia activation, and αSyn pathology. Antibiotic treatment ameliorates, while microbial re-colonization promotes, pathophysiology in adult animals, suggesting that postnatal signaling between the gut and the brain modulates disease. Indeed, oral administration of specific microbial metabolites to germ-free mice promotes neuroinflammation and motor symptoms. Remarkably, colonization of αSyn-overexpressing mice with microbiota from PD-affected patients enhances physical impairments compared to microbiota transplants from healthy human donors. These findings reveal that gut bacteria regulate movement disorders in mice and suggest that alterations in the human microbiome represent a risk factor for PD.

INTRODUCTION

Neurological dysfunction is the basis of numerous human diseases. Behavioral, psychiatric, and neurodegenerative disorders often display hallmark neuropathologies within the central nervous system (CNS). One neuropathology, amyloidosis, results from aberrant aggregation of specific neuronal proteins that disrupt many cellular functions. Affected tissues often contain insoluble aggregates of proteins that display altered conformations, a feature believed to contribute to an estimated 50 distinct human diseases (Sacchettini and Kelly, 2002). Neurodegenerative amyloid disorders, including Alzheimer's, Huntington's, and Parkinson's diseases (PD), are each associated with a distinct amyloid protein (Brettschneider et al., 2015). PD is the second most common neurodegenerative disease in the United States, affecting an estimated 1 million people and 1% of the US population over 60 years of age (Nalls et al., 2014). Worldwide, about 3 million patients and caregivers suffer from the often-debilitating symptoms of PD, which involve motor deficits including tremors, muscle rigidity, bradykinesia, and impaired gait. It is a multifactorial disorder that has a strong environmental component, as less than 10% of cases are hereditary (Nalls et al., 2014). Aggregation of α-synuclein (αSyn) is thought to be pathogenic in a family of diseases termed synucleinopathies, which includes PD, multiple system atrophy, and Lewy body disease (Brettschneider et al., 2015; Luk et al., 2012; Prusiner et al., 2015). αSyn aggregation is a stepwise process, leading to oligomeric species and intransient fibrils that accumulate within neurons. Dopaminergic neurons of the substantia nigra pars compacta (SNpc) appear particularly vulnerable to effects of αSyn aggregates. Dopamine modulators are a first-line therapeutic in PD; however, treatments can carry serious side effects and often lose effectiveness (Jenner, 2008). Discovery of safe and effective therapeutics are needed to address the increasing burden of PD in an ever-aging population, a paradoxical consequence of mankind's achievements in increased lifespan.

Although neurological diseases have been historically studied within the CNS, peripheral influences have been implicated in the

onset and/or progression of diseases that impact the brain (Dinan and Cryan, 2015). Indeed, emerging data suggest bidirectional communication between the gut and the brain in anxiety, depression, nociception, and autism spectrum disorder (ASD), among others (Mayer et al., 2014; Schroeder and Bäckhed, 2016; Sharon et al., 2016). Gastrointestinal (GI) physiology and motility are influenced by signals arising both locally within the gut and from the CNS. Neurotransmitters, immune signaling, hormones, and neuropeptides produced within the gut may, in turn, impact the brain (Selkrig et al., 2014; Wall et al., 2014). Research into how the gut-brain axis influences neurological conditions may reveal insights into disease etiology.

The human body is permanently colonized by microbes on virtually all environmentally exposed surfaces, the majority of which reside within the GI tract (Ley et al., 2006). Increasingly, research is beginning to uncover the profound impacts that the microbiota can have on neurodevelopment and the CNS (Sharon et al., 2016). Germ-free (GF) mice and antibiotic-treated specific-pathogen-free (SPF) mice are altered in hippocampal neurogenesis, resulting in impaired spatial and object recognition (Möhle et al., 2016). The microbiota regulate expression of the 5-hydroxytryptamine receptor (5-HT_{1A}), brain-derived neurotropic factor (BDNF), and NMDA receptor subunit 2 (NR2A) (Bercik et al., 2011; Diaz Heijtz et al., 2011; Sudo et al., 2004). GF mice have altered cortical myelination and impaired blood-brain barrier function (Braniste et al., 2014; Hoban et al., 2016). Additionally, the microbiota promotes enteric and circulating serotonin production in mice (Yano et al., 2015) and affects anxiety, hyperactivity, and cognition (Clarke et al., 2013; Diaz Heijtz et al., 2011; Neufeld et al., 2011; Selkrig et al., 2014). To augment mouse models, dysbiosis (alterations to the microbial composition) of the human microbiome has been reported in subjects diagnosed with several neurological diseases (Schroeder and Bäckhed, 2016). For example, fecal and mucosa-associated gut microbes are different between individuals with PD and healthy controls (Hasegawa et al., 2015; Keshavarzian et al., 2015; Scheperjans et al., 2015; Unger et al., 2016). Yet, how dysbiosis arises and whether this feature contributes to PD pathogenesis remains unknown.

Gut bacteria control the differentiation and function of immune cells in the intestine, periphery, and brain (Erny et al., 2015; Matcovitch-Natan et al., 2016; Rooks and Garrett, 2016). Intriguingly, subjects with PD exhibit intestinal inflammation (Devos et al., 2013), and GI abnormalities such as constipation often precede motor defects by many years (Braak et al., 2003; Verbaan et al., 2007). Braak's hypothesis posits that aberrant αSyn accumulation initiates in the gut and propagates via the vagus nerve to the brain in a prion-like fashion (Del Tredici and Braak, 2008). This notion is supported by pathophysiologic evidence: αSyn inclusions appear early in the enteric nervous system (ENS) and the glossopharyngeal and vagal nerves (Braak et al., 2003; Shannon et al., 2012), and vagotomized individuals are at reduced risk for PD (Svensson et al., 2015). Further, injection of αSyn fibrils into the gut tissue of healthy rodents is sufficient to induce pathology within the vagus nerve and brainstem (Holmqvist et al., 2014). However, the notion that αSyn aggregation initiates in the ENS and spreads to the CNS via retrograde transmission remains controversial (Burke et al., 2008), and experimental support for a gut microbial connection to PD is lacking.

Based on the common occurrence of GI symptoms in PD, dysbiosis among PD patients, and evidence that the microbiota impacts CNS function, we tested the hypothesis that gut bacteria regulate the hallmark motor deficits and pathophysiology of synucleinopathies. Herein, we report that the microbiota is necessary to promote αSyn pathology, neuroinflammation, and characteristic motor features in a validated mouse model. We identify specific microbial metabolites that are sufficient to promote disease symptoms. Remarkably, fecal microbes from PD patients impair motor function significantly more than microbiota from healthy controls when transplanted into mice. Together, these results suggest that gut microbes may play a critical and functional role in the pathogenesis of synucleinopathies such as PD.

RESULTS

Gut Microbes Promote Motor and GI Dysfunction

The Thy1-αSyn (alpha-synuclein-overexpressing [ASO]) mouse displays progressive deficits in fine and gross motor function, as well as gut motility defects (Chesselet et al., 2012; Rockenstein et al., 2002). Recent evidence has linked unregulated αSyn expression in humans to a higher risk of PD (Soldner et al., 2016), providing an epidemiological foundation for the Thy1-αSyn mouse model. Defects in coordinated motor tasks become evident at 12 weeks of age (Fleming et al., 2004). Motor function was measured via four tests: beam traversal, pole descent, nasal adhesive removal, and hindlimb clasping reflexes, as previously validated in this model (Fleming et al., 2004). 12- to 13-week-old ASO animals harboring a complex microbiota (SPF-ASO) require significantly more time to cross a challenging beam compared to wild-type littermates (SPF-WT) and also exhibit increased time to descend a pole, two measures of gross motor function (Figures 1A and 1B). Removal of an adhesive from the nasal bridge, a test of fine motor control, is impaired in SPF-ASO mice compared to SPF-WT mice (Figure 1C). Finally, the hindlimb clasping reflex, a measure of striatal dysfunction (Zhang et al., 2014), is defective in SPF-ASO mice (Figure 1D). To assess the contribution of gut bacteria, we rederived ASO mice (GF-ASO) and wild-type mice (GF-WT) under germ-free conditions. Remarkably, 12- to 13-week-old GF-ASO animals exhibit reduced deficits in beam traversal, pole descent, adhesive removal, and hindlimb clasping (Figures 1A–1D). In fact, the execution of motor function tasks by GF-ASO mice resembles performance levels of WT animals in many cases. GF-ASO mice do not exhibit differences in weight compared to SPF-ASO animals (Figure S1A), while both SPF-ASO and GF-ASO animals display defects in the inverted grid assay, a measure of limb strength (Figure S1B)—thus, outcomes in motor tests are not due to weight or physical strength. At a later age (24–25 weeks old), SPF-ASO animals exhibit a progressive decline in motor function (Figures S1C–S1G), which is significantly delayed in GF-ASO animals (Figures S1C–S1G). We do not observe consistent differences in motor tasks between GF-WT and SPF-WT animals, providing evidence for gene-microbiome interactions.

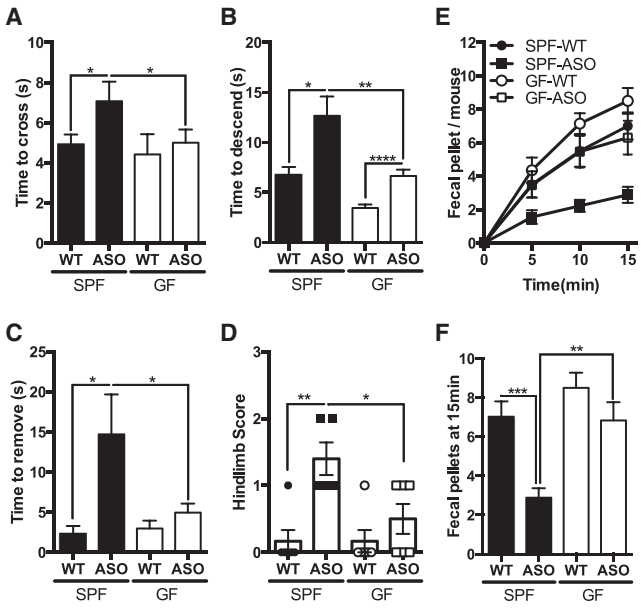

Figure 1. Gut Microbes Promote Motor and Gastrointestinal Dysfunction

(A) Time to traverse beam apparatus.

(B) Time to descend pole.

(C) Time to remove adhesive from nasal bridge.

(D) Hind-limb clasping reflex score.

(E) Time course of fecal output in a novel environment over 15 min.

(F) Total fecal pellets produced in 15 min.

Animals were tested at 12–13 weeks of age. n = 4–6, error bars represent the mean and standard error from three trials per animal. Data are representative of two experiments. *p ≤ 0.05; **p ≤ 0.01; ***p ≤ 0.001; ****p ≤ 0.0001. Abbreviations: SPF, specific-pathogen-free; GF, germ-free; WT, wild-type; ASO, Thy1-α-synuclein genotype. See also Figure S1.

As in PD, motor dysfunction in this mouse model co-occurs with decreased GI function and constipation (Verbaan et al., 2007; Wang et al., 2012). In SPF-ASO animals, we observe a marked decrease in the total output of fecal pellets, at both 12–13 weeks and 24–25 weeks of age, while fecal output is unaltered in GF-ASO animals (Figures 1E, 1F, S1H, and S1I). Further, fecal pellets produced by SPF-ASO mice contain reduced water content compared to GF-ASO mice (Figure S1J), together revealing reduced GI defects in GF animals. Indeed, compilation of all motor phenotypes into a principal-component analysis (PCoA) displays a striking segregation by the SPF-ASO group, while GF-ASO animals cluster more similarly to WT mice (Figure S1K). Together, these data demonstrate that the presence of gut microbes promote the hallmark motor *and* intestinal dysfunction in a preclinical model of PD.

The Gut Microbiota Is Required for αSyn Pathology

Motor deficits in PD coincide with the aggregation of αSyn. Utilizing an antibody that recognizes only conformation-specific αSyn aggregates and fibrils, we performed immunofluorescence microscopy to visualize αSyn inclusions in the brains of mice. Under SPF conditions, we observe notable aggregation of αSyn in the caudoputamen (CP) and substantia nigra (SN) of ASO animals (Figures 2A and 2B), brain regions of the nigrostriatal pathway affected in both mouse models and human PD (Brettschneider et al., 2015). Surprisingly, GF-ASO mice display appreciably fewer αSyn aggregates (Figures 2A and 2B). To quantify αSyn aggregation, we performed western blots of brain extracts (Figure 2C). We reveal significantly less insoluble αSyn in brains of GF-ASO animals (Figures 2C–2E). To further confirm these findings, we performed dot blot analysis for aggregated αSyn in the CP and inferior midbrain, where the SN is located, and observe similarly decreased αSyn aggregation in GF-ASO animals (Figures S2A–S2C). Interestingly, we observe regional specificity of αSyn aggregation: in the frontal cortex (FC), GF-ASO animals harbor fewer αSyn aggregation than SPF animals, while in the cerebellum (CB), we observe nearly equal quantities of αSyn in SPF and GF mice (Figures S2D–S2H). To ensure that these findings do not reflect differences in transgene expression, we report similar levels of αSyn transcript and protein in the inferior midbrain and the CP between SPF- and GF-ASO animals (Figures 2F and 2G). These data suggest that the microbiota regulates pathways that promote αSyn aggregation and/or prevent the clearance of insoluble protein aggregates.

αSyn-Dependent Microglia Activation by the Microbiota

The microbiota modulates immune development in the CNS (Erny et al., 2015; Matcovitch-Natan et al., 2016), and αSyn aggregates activate immune cells, including brain-resident microglia (Kim et al., 2013; Sanchez-Guajardo et al., 2013). Microglia undergo significant morphological changes upon activation, transitioning from thin cell bodies with numerous branched extensions to round, amoeboid cells with fewer branches (Erny et al., 2015). In situ 3D reconstructions of individual microglia cells from confocal fluorescence microscopy reveals that wild-type GF animals harbor microglia that are distinct from SPF animals. Within the CP and SN, microglia in GF-WT mice display increased numbers and total lengths of microglia branches compared to SPF-WT animals (Figures 3A–3C). These morphological features are indicative of an arrest in microglia maturation and/or a reduced activation state in GF animals, corroborating a recent report that gut bacteria affect immune cells in the brain (Erny et al., 2015).

Extending these observations to a disease model, microglia from SPF-ASO mice display significant increases in cell body diameter, along with fewer processes of shorter length compared to GF-ASO mice (Figures 3A–3C). Tissue homogenates from the CP and inferior midbrain of SPF-ASO mice contain a marked increase in the pro-inflammatory cytokines tumor necrosis factor-α (TNF-α) and interleukin-6 (IL-6) compared to GF-ASO mice (Figures 3D and 3E). Both cytokines are elevated in the brains of PD patients (Mogi et al., 1994a, 1994b). Gene expression analysis of RNA from enriched CD11b$^+$ cells (primarily microglia) reveals increased *Tnfa* and *Il6* expression in SPF-ASO animals, which is nearly absent in GF animals (Figure 3F). Neuroprotective *Bdnf* and the cell cycle marker *Ddit4* levels are upregulated in GF animals (Figure S2I), as observed in previous studies (Erny et al., 2015; Matcovitch-Natan et al., 2016). Neuroinflammatory responses are region specific with increased in microglia diameter and TNF-α

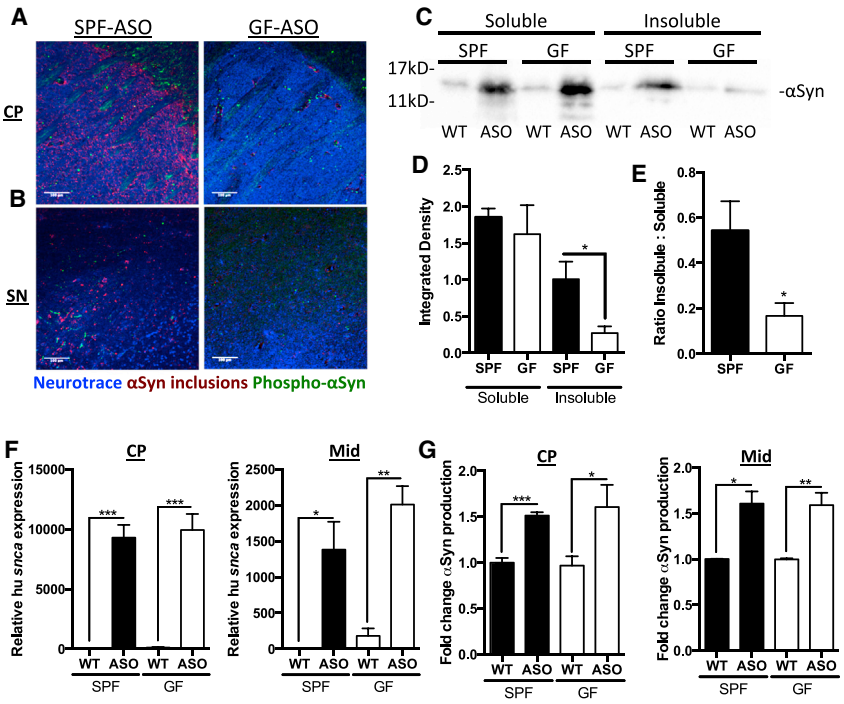

Figure 2. αSyn Pathology Is Increased in Mice Harboring a Gut Microbiota

(A) Representative images of the caudoputamen (CP) from SPF-ASO or GF-ASO animals stained with aggregation-specific αSyn antibody (red), Phospho-Ser129-αSyn antibody (green), and Neurotrace/Nissl (blue).

(B) Representative images of the substantia nigra (SN) from SPF-ASO or GF-ASO animals, stained as above.

(C) Representative western blot of triton soluble and insoluble brain homogenates, immunostained with anti-αSyn antibody.

(D and E) Densitometry quantification of anti-αSyn western blots for (D) all αSyn and (E) ratio of insoluble to soluble αSyn staining.

(F) qRT-PCR analysis of human αSyn in the CP or inferior midbrain (Mid).

(G) ELISA analysis of total αSyn present in homogenates from the CP or inferior midbrain (Mid).

Tissues collected from mice at 12–13 weeks of age. n = 3–4, error bars represent the mean and standard error. *p ≤ 0.05; **p ≤ 0.01; ***p ≤ 0.001. Abbreviations: SPF, specific-pathogen-free; GF, germ-free; WT, wild-type; ASO, Thy1-α-synuclein genotype. See also Figure S2.

production in the FC but not the CB (Figures 3G and 3H). Overall, these findings support the hypothesis that gut microbes promote αSyn-dependent activation of microglia within specific brain regions involved in disease.

Postnatal Microbial Signals Modulate αSyn-Dependent Pathophysiology

The microbiota influence neurological outcomes during gestation, as well as via active gut-to-brain signaling in adulthood. In order to differentiate between these mechanisms, we treated SPF animals with an antibiotic cocktail to postnatally deplete the microbiota (Figure 4A). Conversely, we colonized groups of 5- to 6-week-old GF mice with a complex microbiota from SPF-WT animals (Figure 4A). Remarkably, antibiotic-treated (Abx) animals display little αSyn-dependent motor dysfunction, closely resembling mice born under GF conditions (Figures 4B–4E). Postnatal colonization of previously GF animals (Ex-GF) recapitulates the genotype effect observed in SPF mice, with mice that overexpress αSyn displaying significant motor dysfunction (Figures 4B–4E). GI function, as measured by fecal output, is also significantly improved in Abx-treated animals, while Ex-GF mice exhibit an αSyn-dependent decrease in total fecal output (Figures 4F and 4G). Furthermore, in the transgenic ASO line, microglia from Ex-GF animals have increased cell body diameters comparable to those in SPF mice (Figures 4H and 4I). Abx-ASO animals, however, harbor microglia with diameters similar to GF animals (Figures 4H and 4I). While not excluding a role for the microbiota during prenatal neurodevelopment, modulation of microglia activation during adulthood contributes to αSyn-mediated motor dysfunction and neuroinflammation, suggesting active gut-brain signaling by the microbiota.

SCFAs Are Sufficient to Promote αSyn-Mediated Neuroinflammation

Recently, it was revealed that gut bacteria modulate microglia activation during viral infection through production of microbial metabolites, namely short-chain fatty acids (SCFAs) (Erny et al., 2015). Indeed, we observe lower fecal SCFA concentrations in GF and Abx-treated animals, compared to SPF mice (Figure S3A; Smith et al., 2013). To address whether SCFAs impact neuroimmune responses in a mouse model of PD, we treated GF-ASO and GF-WT animals with a mixture of the SCFAs acetate, propionate, and butyrate (while the animals remained microbiologically sterile) and significantly restored fecal SCFA concentrations (Figure S3A). Within affected brain regions (i.e., CP and SN), microglia in SCFA-administered animals display morphology indicative of increased activation compared to untreated mice, and similar to cells from Ex-GF and SPF mice (Figures 5A, 5B, S3B, and S3C; see also Figures 3 and 4). Microglia from GF-ASO mice fed SCFAs (SCFA-ASO) are significantly larger in diameter than those of GF-WT animals treated with SCFAs (SCFA-WT), with a concomitant decrease in the length and total number of branches. Abx-treated animals, however, display microglia morphology similar to GF animals (Figures 5B, S3B, and S3C; see also Figures 3 and 4). Changes in microglia diameter are also observed in the FC, but not the CB, demonstrating region-specific responses (Figures S3D and S3E).

Corresponding to microglia morphology, we reveal αSyn aggregates in mice administered SCFAs compared to untreated and Abx-treated mice, and similar to Ex-GF animals (Figures S3F–S3I). Strikingly, we observe that postnatal signaling by microbes induces increased αSyn aggregation in the CP and SN (Figures S3F and S3G), with no observable difference in the FC and CB (Figures S3H and S3I), confirmed by quantification and

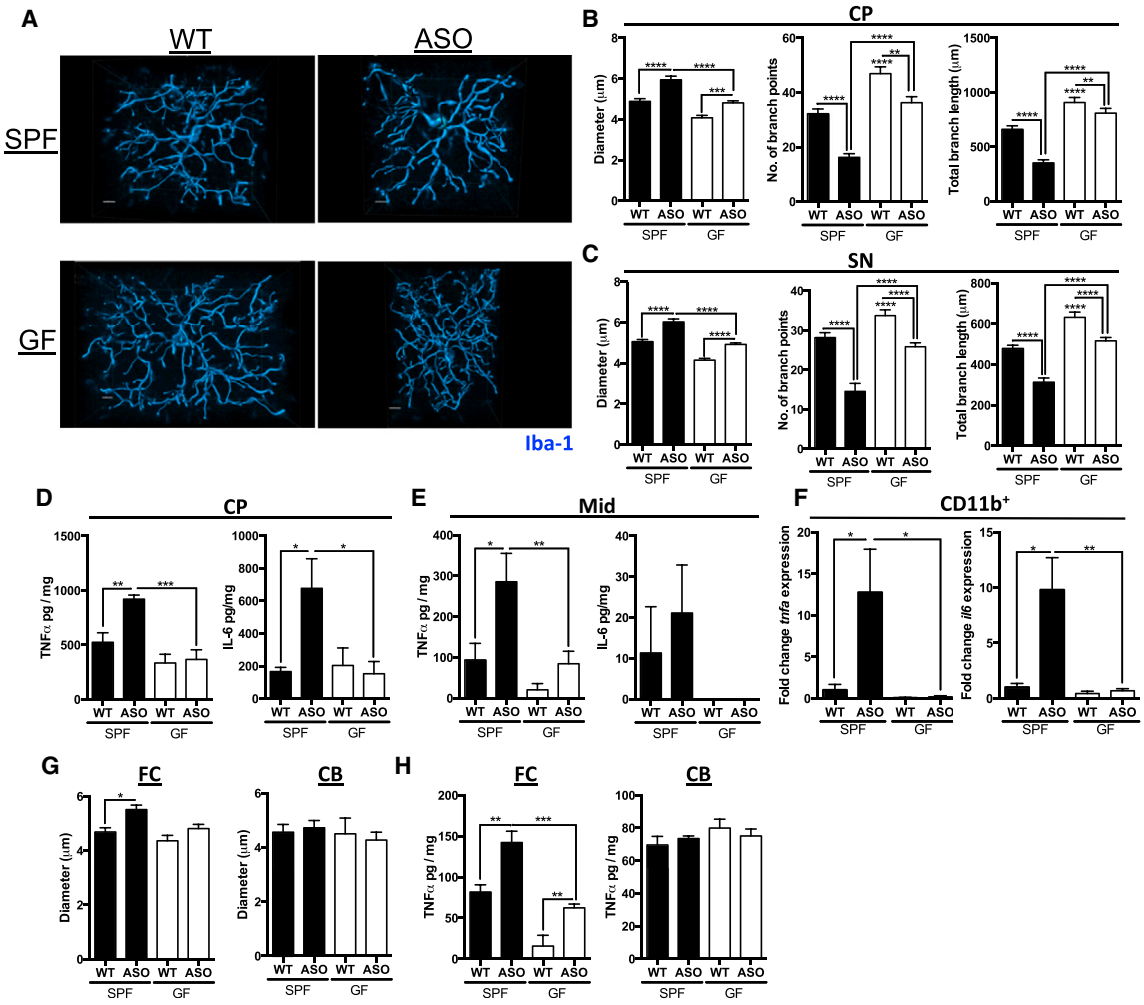

Figure 3. αSyn-Dependent Microglia Activation by the Microbiota

(A) Representative 3D reconstructions of Iba1-stained microglia residing in the caudoputamen (CP) of SPF-WT, SPF-ASO, GF-WT, and GF-ASO animals.

(B) CP-resident microglia parameters diameter, number of branch points, and total branch length.

(C) Substantia nigra (SN)-resident microglia parameters diameter, number of branch points, and total branch length.

(D) ELISA analysis for TNF-α and IL-6 present in homogenates from the CP.

(E) ELISA analysis for TNF-α and IL-6 present in homogenates from the inferior midbrain (Mid).

(F) qPCR analysis of CD11b$^+$ cells derived from brain homogenate for *tnfa* and *il6*.

(G) Diameter of microglia residing in the frontal cortex (FC) or cerebellum (CB).

(H) ELISA analysis for TNF-α present in homogenates from the FC or CB.

Tissues collected from mice at 12–13 weeks of age. n = 3–4 (with 20–60 cells per region per animal analyzed); error bars represent the mean and standard error. *p ≤ 0.05; **p ≤ 0.01; ***p ≤ 0.001; ****p ≤ 0.0001. Abbreviations: SPF, specific-pathogen-free; GF, germ-free; WT, wild-type; ASO, Thy1-α-synuclein genotype. See also Figure S2.

western blot (Figures S3J–S3O). SCFAs either singly or in a mixture, over a range of concentrations, do not expedite the aggregation of human αSyn in vitro (Figures S4A–S4G), nor do they alter the overall structure of αSyn amyloid fibrils (Figures S4H and S4I). Though additional studies are needed, it appears that SCFAs accelerate in vivo αSyn aggregation, albeit independently of direct molecular interactions.

SCFAs Are Sufficient to Promote Motor Deficits

To explore a link between microbial metabolites and motor symptoms in the Thy1-αSyn model, GF animals were treated with the SCFA mixture beginning at 5–6 weeks of age, and motor function was assessed at 12–13 weeks of age. SCFA-ASO mice display significantly impaired performance in several motor tasks compared to untreated GF-ASO animals (Figures 5C–5F), including impairment in beam traversal, pole descent, and hindlimb reflex (compare GF-ASO to SCFA-ASO mice). All effects by SCFAs are genotype specific to the Thy1-αSyn mice. GI deficits are also observed in the SCFA-treated transgenic animals (Figures 5G and 5H). Oral treatment of GF animals with heat-killed bacteria does not induce motor deficits (Figures S4J–S4M), suggesting that bacteria need to be metabolically

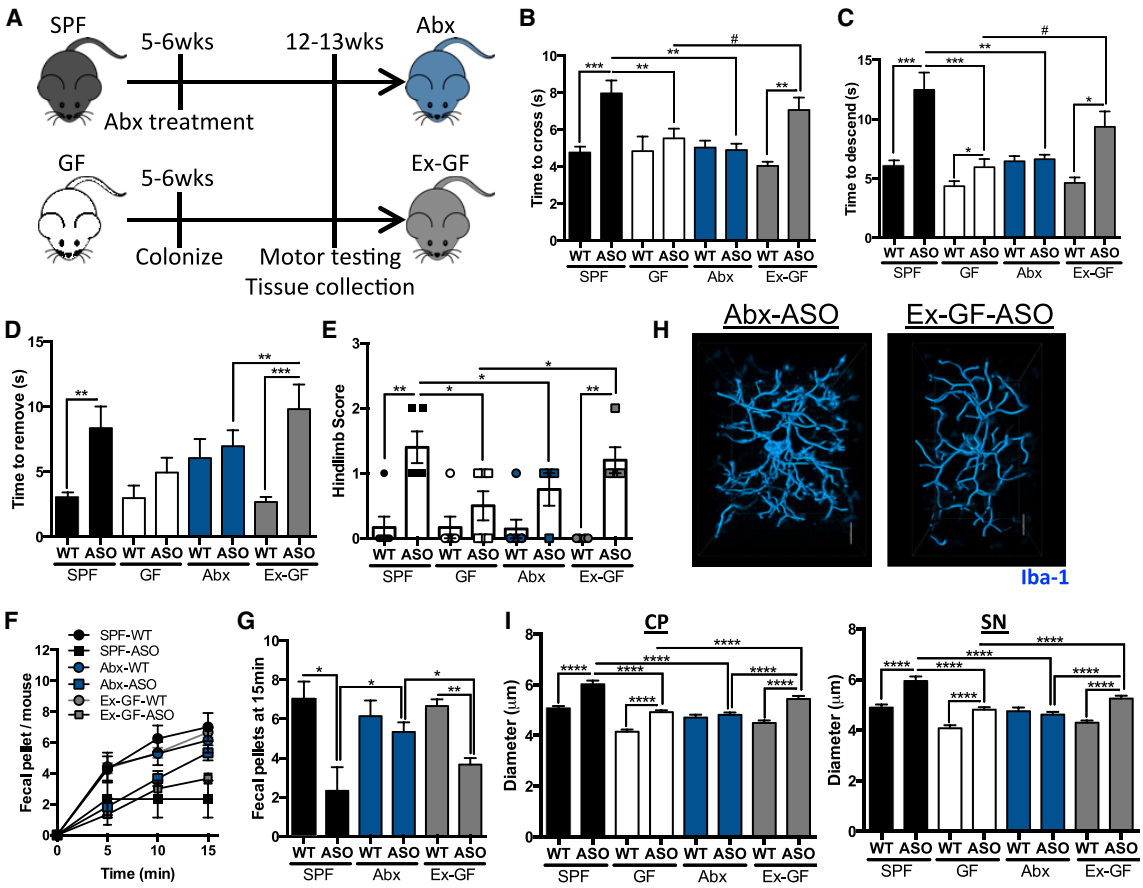

Figure 4. Postnatal Microbial Signals Promote Motor and Gastrointestinal Dysfunction

(A) Time course schema for animal treatment and testing.

(B) Time to traverse beam apparatus.

(C) Time to descend pole.

(D) Time to remove nasal adhesive.

(E) Hindlimb clasping reflex score.

(F) Time course of fecal output in a novel environment over 15 min.

(G) Total fecal pellets produced in 15 min.

(H) Representative 3D reconstructions of Iba1-stained microglia residing in the caudoputamen (CP) of Abx-ASO or Ex-GF-ASO animals.

(I) Diameter of microglia residing in the CP or substantia nigra (SN).

Animals were tested at 12–13 weeks of age. n = 6–12; error bars represent the mean and standard error from 3 trials per animal, and compiled from 2 independent cohorts or 20–60 microglia per region analyzed. $^{\#}0.05 < p < 0.1$; $^{*}p \leq 0.05$; $^{**}p \leq 0.01$; $^{***}p \leq 0.001$; $^{****}p \leq 0.0001$. Abbreviations: SPF, specific-pathogen-free; GF, germ-free; Abx, antibiotic-treated; Ex-GF, recolonized germ-free animals; WT, wild-type; ASO, Thy1-α-synuclein genotype. See also Figure S3.

active. Additionally, oral treatment of SCFA-fed animals with the anti-inflammatory compound minocycline is sufficient to reduce TNF-α production, reduce αSyn aggregation, and improve motor function, without altering transgene expression (Figures S5A–S5H). We propose that the microbiota actively produce metabolites, such as SCFAs, that are required for microglia activation and αSyn aggregation, contributing to motor dysfunction in a preclinical model of PD.

Dysbiosis of the PD Microbiome

Given recent evidence that PD patients display altered microbiomes (Hasegawa et al., 2015; Keshavarzian et al., 2015; Scheperjans et al., 2015), we sought to determine whether human gut microbes affect disease outcomes when transferred into GF mice. We collected fecal samples from six human subjects diagnosed with PD as well as six matched healthy controls (Table S1). To limit confounding effects, only new-onset, treatment-naive PD patients with healthy intestinal histology were chosen, among other relevant inclusion and exclusion criteria (see STAR Methods and Table S1).

Fecal microbiota from PD patients or controls were transplanted into individual groups of GF recipient animals via oral gavage. Fecal pellets were collected from "humanized" mice, bacterial DNA was extracted, and 16S rRNA sequencing was performed. Sequences were annotated into operational taxonomic units (OTUs), using closed reference picking against the Greengenes database and metagenome function was predicted by PICRUSt. Recipient animal groups were most similar to their

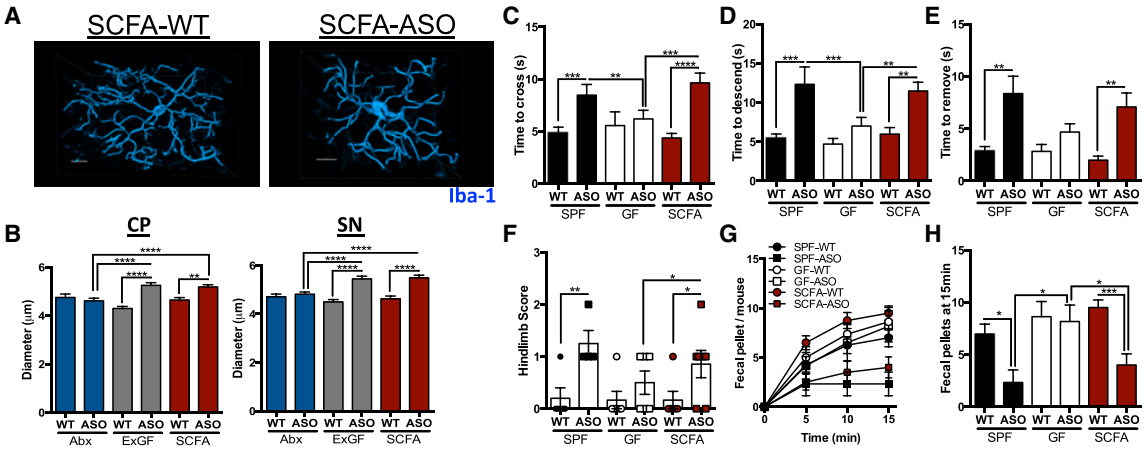

Figure 5. SCFAs Promote αSyn-Stimulated Microglia Activation and Motor Dysfunction

(A) Representative 3D reconstructions of Iba1-stained microglia residing in the caudoputamen (CP) of wild-type or ASO SCFA-treated animals.

(B) Diameter of microglia residing in the CP or substantia nigra (SN).

(C) Time to traverse beam apparatus.

(D) Time to descend pole.

(E) Time to remove nasal adhesive.

(F) Hindlimb clasping reflex score.

(G) Time course of fecal output in a novel environment over 15 min.

(H) Total fecal pellets produced in 15 min.

Animals were tested at 12–13 weeks of age. n = 6–12, error bars represent the mean and standard error from 3 trials per animal, and compiled from 2 independent cohorts or 20–60 microglia per region analyzed. Data are plotted with controls from Figure 4 for clarity. *p ≤ 0.05; **p ≤ 0.01; ***p ≤ 0.001; ****p ≤ 0.0001. Abbreviations: SPF, specific-pathogen-free; GF, germ-free; SCFA, short-chain fatty acid-treated; WT, wild-type; ASO, Thy1-α-synuclein genotype. See also Figures S3, S4, and S5.

respective human donor's profile in unweighted UniFrac (Lozupone and Knight, 2005), based on PCoA (Figures 6A and 6B). Strikingly, the disease status of the donor had a strong effect on the microbial communities within recipient mice. Humanized mouse groups from PD donors are significantly more similar to each other than to communities transplanted from healthy donors, with this trend persisting when stratified by genetic background (Figures 6C and 6D). Furthermore, there are significant differences between the healthy and PD donors in the ASO background compared to WT recipients, suggesting genotype effects on microbial community configuration (Figures 6C and 6D).

We identified a number of genera that are altered in animals colonized with microbiota derived from PD donors, compared to healthy controls (Figure 6E), as well as altered KEGG pathways between these groups as indicated by Bray-Curtis distances (Figures S6A–S6C). OTUs increased in abundance in mice with PD microbiomes include *Proteus* sp., *Bilophila* sp., and *Roseburia* sp., with a concomitant loss of members of families Lachnospiraceae, Rikenellaceae, and Peptostreptococcaceae, as well as *Butyricicoccus* sp. (Figure 6E). Interestingly, some taxa are altered only in ASO animals (e.g., *Proteus* sp., *Bilophila* sp., and Lachnospiraceae), while others display significant changes independent of mouse genotype (e.g., *Roseburia* sp., Rikenellaceae, and *Enterococcus* sp.) (Figure 6E). Intriguingly, the abundance of three SCFA-producing KEGG families (K00929, butyrate kinase, and K01034 and K01035, acetate CoA/acetoacetate CoA transferase alpha and beta) are increased in mice that received fecal microbes derived from PD donors (Figure S6D). Further, we observe that animals receiving PD donor-derived microbiota display a significantly altered SCFA profile, with a lower concentration of acetate and higher relative abundances of propionate and butyrate, compared to animals colonized with microbes from healthy controls (Figure S6E). Together, these data indicate that differences in fecal microbial communities between PD patients and controls can be maintained after transfer into mice. Further, αSyn overexpression engenders distinct alterations to the gut microbiome profile after transplantation.

PD-Derived Gut Microbiota Promotes Motor Dysfunction

To assess microbiota function, groups of humanized animals from each of the donor pairs were tested for motor function. Consistent among four of the six pairs (pairs #1, 3, 4, and 5), microbiota derived from individuals with PD promote increased αSyn-mediated motor dysfunction (Figures 7A–7F). Beam traversal, pole descent, and nasal adhesive removal are significantly impaired in ASO animals colonized with PD microbiota compared to genotype-matched recipient mice harboring gut bacteria from healthy controls. Hindlimb reflex scores, on the other hand, are generally not different between individual donors. Interestingly, microbiota from one pair of samples did not induce significant genotype effects in the beam traversal and pole descent tasks (pair #2, Figure 7B), reflecting potential heterogeneity in the population that needs to be addressed through well-powered cohort studies. We observed no notable effects in motor function by WT recipient animals colonized with microbiota from either donor group (Figures 7A–7F). This finding in a

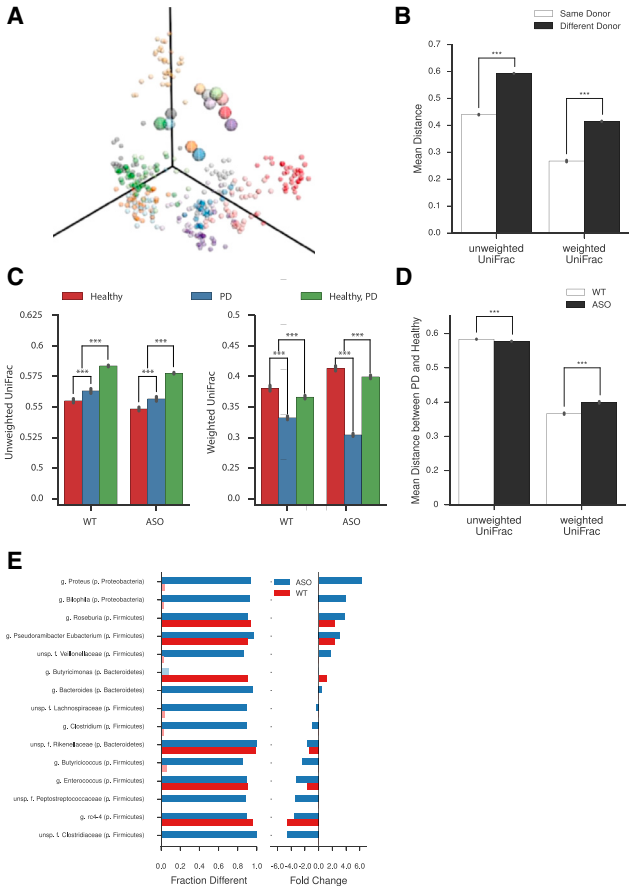

Figure 6. Microbiome Dysbiosis of PD Patient Samples after Transplant into Germ-free Mice

(A) Unweighted UniFrac Principle Coordinate Analysis of microbial communities of human donors (large circles) and recipient mice (small circles). Each donor and recipient sample are matched by color.

(B) Unweighted and weighted UniFrac analysis of microbial communities in recipient animals based on donor identity.

(C) Unweighted and weighted UniFrac analysis of microbial communities in recipient animals based on mouse genotype.

(D) Comparison of unweighted and weighted UniFrac analysis of microbial communities in recipient animals.

(E) Taxa-level analysis of individual genera altered between PD and healthy donors as a function of recipient mouse genotype. Left column indicates percentage with significant differences observed; right column indicates fold change between PD and healthy donors. Light colors indicate non-statistically significant differences.

n = 3–6, over 3 time points post-colonization. Error bars represent the mean and standard error. ***$p \leq 0.001$, 999 permutations. Abbreviations: HC, germ-free mice colonized with fecal microbes from healthy controls; PD, germ-free mice colonized with fecal microbes from Parkinson's disease patients; WT, wild-type; ASO, Thy1-α-synuclein genotype. See also Figure S6.

preclinical mouse model supports the notion the PD microbiota contributes to disease symptoms in genetically susceptible hosts. Notably, recipient animals display little alteration to weight and GI function as measured by fecal output (Figures S7A–S7F). Compilation of performance data from all groups reveals that microbiota from PD patients induce increased motor impairment in ASO animals compared to microbes from healthy controls in three of four tests used in this study (Figure 7G). In fact, depicting all motor function by PCoA displays striking global differences between animals colonized with microbiota from PD donors, compared to those colonized with gut bacteria derived from healthy individuals (Figure S7G). The observation that gut bacteria from PD patients compared to healthy controls enhance motor deficits in a mouse model provides evidence for a functional contribution by the microbiota to synuclienopathies.

DISCUSSION

Parkinson's disease represents a growing health concern for an ever-aging population. While genetic risks have been identified, environmental factors and gene-environment interactions probably account for most PD cases (Nalls et al., 2014; Ritz et al., 2016). We provide evidence that the gut microbiota are required for postnatal events that promote hallmark motor deficits in an animal model. Under GF conditions, or when bacteria are depleted with antibiotics, transgenic animals overexpressing human αSyn display reduced microglia activation, αSyn inclusions, and motor deficits compared to animals with a complex microbiota. Treatment with microbially produced SCFAs restores all major features of disease in GF mice, identifying potential molecular mediators involved in gut-brain signaling. Exacerbated motor symptoms in humanized mice transplanted with a PD microbiota compared to healthy controls suggest that αSyn overexpression (genetics) and dysbiosis (environment) combine to influence disease outcomes in mice. Extrapolation of these preclinical findings to humans may embolden the concept that gene-microbiome interactions represent a previously unrecognized etiology for PD.

Mechanisms by which gut bacteria promote αSyn-mediated pathophysiology are likely complex; herein, we have identified one potential pathway requiring microbiota-dependent effects on microglia. Recent studies have demonstrated an active role for the gut microbiota in promoting full maturation and inflammatory capabilities of microglia through the production of SCFAs (Erny et al., 2015). Despite a requirement for the SCFA receptor FFAR2 for microglia maturation, these cells are not known to express FFAR2, but do express other SCFA-responsive genes such as the histone deactylases that modulate gene expression (Erny et al., 2015). SCFAs may cross the BBB and impact the physiology of cells in the CNS (Mitchell et al., 2011), or they may have peripheral effects, which indirectly activate and mature microglia by currently unknown mechanisms (Erny et al., 2015). Further, insoluble aggregates and oligomeric forms of αSyn activate microglia (Kim et al., 2013; Sanchez-Guajardo et al., 2013). Increases in the activation state of microglia and the production of pro-inflammatory cytokines alter neuronal function and increase cell death in models of PD and other neurodegenerative diseases (Kannarkat et al., 2013; Sanchez-Guajardo et al., 2013). Intriguingly, an inflammatory environment is known to enhance αSyn aggregation, which may further activate microglia upon contact and promote a feed-forward cascade that leads to additional αSyn aggregation and propagation and progression of disease (Gao et al., 2011). If true, possible future treatment options may include targeting immune activation by the microbiota, a notion consistent with research

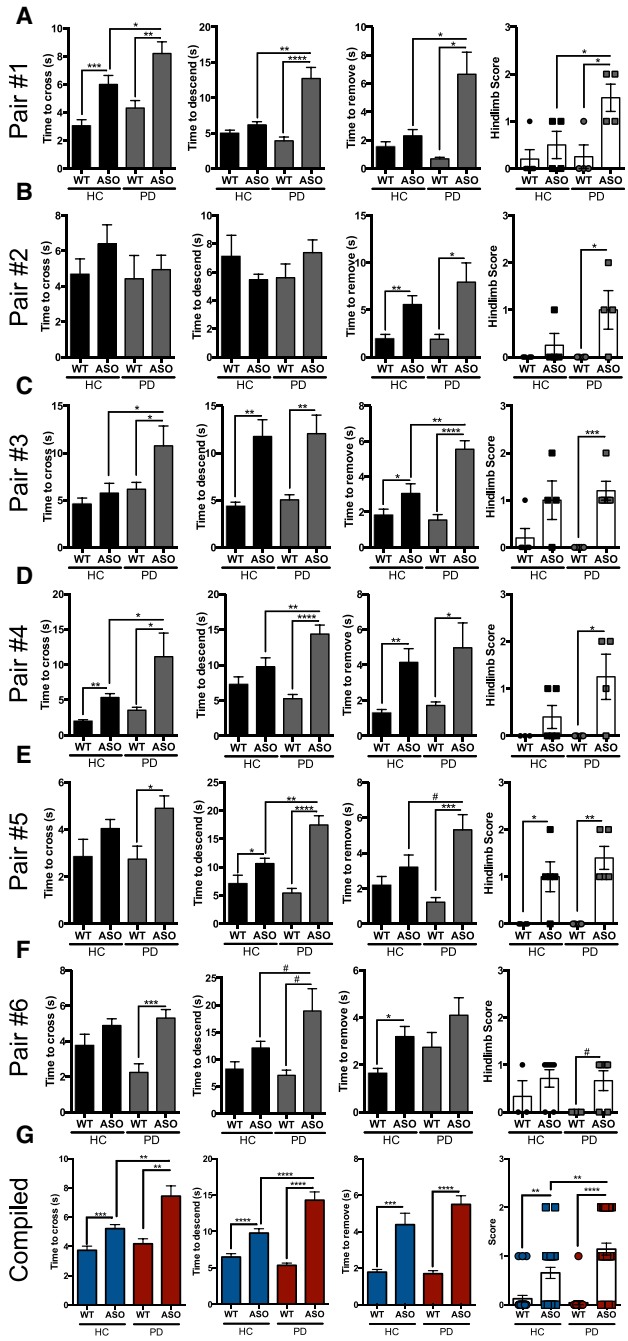

Figure 7. Microbiota from PD Patients Induce Increased αSyn-Mediated Motor Deficits

(A–F) Time to cross a beam, time to descend the pole, time to remove nasal adhesive, and hindlimb clasping reflex scores of mice humanized with microbiota from either PD patients or matched healthy controls.

(G) Compilation of all independent cohorts in each motor task: beam traversal, pole descent, adhesive removal, and hindlimb clasping reflex score, grouped by health status of fecal donor.

Animals were tested at 12–13 weeks of age. n = 3–6, error bars represent the mean and standard error from 3 trials per animal. $^{\#}0.05 < p < 0.1$; *$p \leq 0.05$; **$p \leq 0.01$; ***$p \leq 0.001$; ****$p \leq 0.0001$. Abbreviations: HC, germ-free mice colonized with fecal microbes from healthy controls; PD, germ-free mice colonized with fecal microbes from Parkinson's disease patients; WT, wild-type; ASO, Thy1-α-synuclein genotype. See also Figure S7 and Table S1.

into anti-inflammatory therapeutic modalities for PD (Valera and Masliah, 2016).

While the microbiota promote microglia maturation, there are likely other disease-modifying processes that remain undiscovered. These include effects by the microbiota on autophagy (Lin et al., 2014), a cellular recycling process that is genetically linked to PD risk and when impaired may lead to reduced clearance of αSyn aggregates (Beilina and Cookson, 2015; Nalls et al., 2014). Additionally, intestinal bacteria have been shown to modulate proteasome function (Cleynen et al., 2014), which may also aid in the clearance of αSyn inclusions. The protective effects of autophagy and the proteasome are not specific to synucleinopathies, and the ability of the microbiota to modulate these critical cellular functions suggests that other amyloid disorders, such as Alzheimer's and Huntington's diseases, may be impacted by gut bacteria. In fact, recent studies have implicated the gut microbiota in promoting amyloid beta pathology in a model of Alzheimer's disease (Minter et al., 2016). Though we have explored postnatal effects of the microbiota in a model of neurodegenerative disease, our findings do not address the likely important role of microbial signals during prenatal neurodevelopment. Whether gut microbes alter the development of the dopaminergic system, perhaps by modulating neurogenesis or neural differentiation in utero or early life, remains unexplored. Furthermore, gut microbes can produce dopamine and its precursors from dietary substrates, with almost half of the body's dopamine generated in the GI tract (Eisenhofer et al., 1997; Wall et al., 2014). Deciphering microbiota effects on microglia activation, cellular protein clearance pathways, neurotransmitter production, and/or other mechanisms may offer an integrated approach to understand the pathogenesis of a complex and enigmatic disorder such as PD.

We reveal that gut bacteria from PD patients promote enhanced motor impairment compared to microbiota from healthy controls when transplanted into genetically susceptible ASO mice. This surprising finding suggests that distinct microbes associated with PD, rather than general microbial stimulation, manifest disease symptoms. Several bacterial taxa are altered in mice receiving fecal transplants from PD patients compared to healthy controls. Additionally, a number of bacterial genera are changed specifically in ASO animals, but not WT mice, receiving microbes from the same donor. These include depletions in members of family Lachnospiraceae and Ruminococceae in recipient mice, a notable finding as these same genera are significantly reduced in fecal samples directly from PD patients (Keshavarzian et al., 2015). Conversely, the gut microbiomes in human subjects with PD contain an increased abundance of Proteobacteria (Hasegawa et al., 2015; Keshavarzian et al., 2015; Scheperjans et al., 2015; Unger et al., 2016), remarkably similar to our results in mice. Whether these specific microbes play a role in disease processes remains unknown. Intriguingly, a recent study demonstrated alterations in fecal SCFA ratios between patients and healthy controls, including an elevated relative concentration of butyrate, possibly

implicating a role for SCFAs in PD (Unger et al., 2016). Accordingly, we observe altered SCFA abundances in animals colonized with PD donor-derived microbiota, and the discovery that SCFAs are sufficient to generate αSyn-reactive microglia in the brain is consistent with expansive literature showing that altered microbial communities impact immune responses in the gut and periphery (Hooper et al., 2012).

What causes dysbiosis in PD? Physiological functions in affected individuals, such as altered intestinal absorption, reduced gastric motility, or dietary habits, represent factors that may change the microbiome. Epidemiological evidence has linked specific pesticide exposure to the incidence of PD (Ritz et al., 2016), with some pesticides known to impact microbiome configuration (Gao et al., 2016). Given the structure of αSyn and its ability to associate with membranes (Jo et al., 2000), it is tempting to speculate that extracellular αSyn may act as an antimicrobial, similar to recent observations with amyloid beta (Kumar et al., 2016), and shape the PD microbiome. Whether microbial community alterations are caused by extrinsic or intrinsic factors, the PD microbiota may be missing or reduced in protective microbes, harbor increased pathogenic resident microbes, or both. In turn, dysbiosis will result in differential production of microbial molecules in the gut. Metabolites produced by a deranged microbiota may enter the circulation (or even the brain) and impact neurological function. Identification of bacterial taxa or microbial metabolites that are altered in PD may serve as disease biomarkers or even drug targets, and interventions that correct dysbiosis may provide safe and effective treatments to slow or halt the progression of often debilitating motor symptoms.

Our findings establish that the microbiota are required for the hallmark motor and GI dysfunction in a mouse model of PD, via postnatal gut-brain signaling by microbial molecules that impact neuroinflammation and αSyn aggregation. Coupled with emerging research that has linked gut bacteria to disorders such as anxiety, depression, and autism, we propose the provocative hypothesis that certain neurologic conditions that have classically been studied as disorders of the brain may also have etiologies in the gut.

STAR★METHODS

Detailed methods are provided in the online version of this paper and include the following:

- KEY RESOURCES TABLE
- CONTACT FOR REAGENT AND RESOURCE SHARING
- EXPERIMENTAL MODEL AND SUBJECT DETAILS
  - Mice
  - Human Donor and Criteria
- METHOD DETAILS
  - Motor Function and Gastrointestinal Testing
  - Immunostaining and Microglia Reconstructions
  - CD11b Enrichment and qPCR Analysis
  - Cytokine and αSyn ELISAs and Western Blots
  - αSyn Aggregation Assays
  - SCFA Extraction and Analysis
  - Microbiome Profiling
- QUANTIFICATION AND STATISTICAL ANALYSIS
- DATA AND SOFTWARE AVAILABILITY

SUPPLEMENTAL INFORMATION

Supplemental Information includes seven figures and one table and can be found with this article online at http://dx.doi.org/10.1016/j.cell.2016.11.018.

AUTHOR CONTRIBUTIONS

Conceptualization, T.R.S., C.E.S., M.-F.C., and S.K.M.; Formal Analysis, J.W.D., S.J., and C.C.; Investigation, T.R.S., T.T., G.G.S., Z.E.I., and S.R.; Resources, A.K. and K.M.S.; Writing - Original Draft, T.R.S. and S.K.M.; Writing - Review and Editing, all authors; Supervision, V.G., R.K.-B., P.W.-S., R.K., and S.K.M.; Funding Acquisition, T.R.S., V.G., M.-F.C., A.K., P.W.-S., R.K., and S.K.M.

ACKNOWLEDGMENTS

We thank E. Hsiao, M. Sampson, and the S.K.M. laboratory for helpful critiques. We are grateful to K. Ly, A. Maskell, and M. Quintos for animal husbandry and Y. Garcia-Flores, G. Ackermann, G. Humphrey, and H. Derderian for technical support. Imaging and analysis was performed in the Caltech Biological Imaging Facility, with the support of the Caltech Beckman Institute and the Arnold and Mabel Beckman Foundation. T.R.S. is a Larry L. Hillblom Foundation postdoctoral fellow. This project was supported by funds from the Knut and Alice Wallenberg Foundation and Swedish Research Council to P.W.-S.; a gift from Mrs. and Mr. Larry Field to A.K.; the Heritage Medical Research Institute to V.G. and S.K.M.; and NIH grant NS085910 to S.K.M.

Received: June 29, 2016
Revised: October 12, 2016
Accepted: November 10, 2016
Published: December 1, 2016

REFERENCES

Beilina, A., and Cookson, M.R. (2015). Genes associated with Parkinson's disease: regulation of autophagy and beyond. J. Neurochem. *139* (*Suppl 1*), 91–107.

Bercik, P., Denou, E., Collins, J., Jackson, W., Lu, J., Jury, J., Deng, Y., Blennerhassett, P., Macri, J., McCoy, K.D., et al. (2011). The intestinal microbiota affect central levels of brain-derived neurotropic factor and behavior in mice. Gastroenterology *141*, 599–609, 609.e1–609.e3.

Braak, H., Rüb, U., Gai, W.P., and Del Tredici, K. (2003). Idiopathic Parkinson's disease: possible routes by which vulnerable neuronal types may be subject to neuroinvasion by an unknown pathogen. J Neural Transm (Vienna) *110*, 517–536.

Braniste, V., Al-Asmakh, M., Kowal, C., Anuar, F., Abbaspour, A., Tóth, M., Korecka, A., Bakocevic, N., Ng, L.G., Kundu, P., et al. (2014). The gut microbiota influences blood-brain barrier permeability in mice. Sci. Transl. Med. *6*, 263ra158.

Brettschneider, J., Del Tredici, K., Lee, V.M., and Trojanowski, J.Q. (2015). Spreading of pathology in neurodegenerative diseases: a focus on human studies. Nat. Rev. Neurosci. *16*, 109–120.

Burke, R.E., Dauer, W.T., and Vonsattel, J.P. (2008). A critical evaluation of the Braak staging scheme for Parkinson's disease. Ann. Neurol. *64*, 485–491.

Caporaso, J.G., Kuczynski, J., Stombaugh, J., Bittinger, K., Bushman, F.D., Costello, E.K., Fierer, N., Peña, A.G., Goodrich, J.K., Gordon, J.I., et al. (2010). QIIME allows analysis of high-throughput community sequencing data. Nat. Methods *7*, 335–336.

Chesselet, M.F., Richter, F., Zhu, C., Magen, I., Watson, M.B., and Subramaniam, S.R. (2012). A progressive mouse model of Parkinson's disease: the Thy1-aSyn ("Line 61") mice. Neurotherapeutics *9*, 297–314.

Chorell, E., Andersson, E., Evans, M.L., Jain, N., Götheson, A., Åden, J., Chapman, M.R., Almqvist, F., and Wittung-Stafshede, P. (2015). Bacterial chaperones CsgE and CsgC differentially modulate human α-synuclein amyloid formation via transient contacts. PLoS ONE *10*, e0140194.

Clarke, G., Grenham, S., Scully, P., Fitzgerald, P., Moloney, R.D., Shanahan, F., Dinan, T.G., and Cryan, J.F. (2013). The microbiome-gut-brain axis during early life regulates the hippocampal serotonergic system in a sex-dependent manner. Mol. Psychiatry *18*, 666–673.

Cleynen, I., Vazeille, E., Artieda, M., Verspaget, H.W., Szczypiorska, M., Bringer, M.A., Lakatos, P.L., Seibold, F., Parnell, K., Weersma, R.K., et al. (2014). Genetic and microbial factors modulating the ubiquitin proteasome system in inflammatory bowel disease. Gut *63*, 1265–1274.

Del Tredici, K., and Braak, H. (2008). A not entirely benign procedure: progression of Parkinson's disease. Acta Neuropathol. *115*, 379–384.

Devos, D., Lebouvier, T., Lardeux, B., Biraud, M., Rouaud, T., Pouclet, H., Coron, E., Bruley des Varannes, S., Naveilhan, P., Nguyen, J.M., et al. (2013). Colonic inflammation in Parkinson's disease. Neurobiol. Dis. *50*, 42–48.

Diaz Heijtz, R., Wang, S., Anuar, F., Qian, Y., Björkholm, B., Samuelsson, A., Hibberd, M.L., Forssberg, H., and Pettersson, S. (2011). Normal gut microbiota modulates brain development and behavior. Proc. Natl. Acad. Sci. USA *108*, 3047–3052.

Dinan, T.G., and Cryan, J.F. (2015). The impact of gut microbiota on brain and behaviour: implications for psychiatry. Curr. Opin. Clin. Nutr. Metab. Care *18*, 552–558.

Eisenhofer, G., Aneman, A., Friberg, P., Hooper, D., Fåndriks, L., Lonroth, H., Hunyady, B., and Mezey, E. (1997). Substantial production of dopamine in the human gastrointestinal tract. J. Clin. Endocrinol. Metab. *82*, 3864–3871.

Erny, D., Hrabě de Angelis, A.L., Jaitin, D., Wieghofer, P., Staszewski, O., David, E., Keren-Shaul, H., Mahlakoiv, T., Jakobshagen, K., Buch, T., et al. (2015). Host microbiota constantly control maturation and function of microglia in the CNS. Nat. Neurosci. *18*, 965–977.

Fleming, S.M., Salcedo, J., Fernagut, P.O., Rockenstein, E., Masliah, E., Levine, M.S., and Chesselet, M.F. (2004). Early and progressive sensorimotor anomalies in mice overexpressing wild-type human alpha-synuclein. J. Neurosci. *24*, 9434–9440.

Gao, H.M., Zhang, F., Zhou, H., Kam, W., Wilson, B., and Hong, J.S. (2011). Neuroinflammation and α-synuclein dysfunction potentiate each other, driving chronic progression of neurodegeneration in a mouse model of Parkinson's disease. Environ. Health Perspect. *119*, 807–814.

Gao, B., Bian, X., Mahbub, R., and Lu, K. (2016). Gender-specific effects of organophosphate diazinon on the gut microbiome and its metabolic functions. Environ. Health Perspect. Published online May 20, 2016. http://dx.doi.org/10.1289/EHP202.

Gilbert, J.A., Jansson, J.K., and Knight, R. (2014). The Earth Microbiome project: successes and aspirations. BMC Biol. *12*, 69.

Hasegawa, S., Goto, S., Tsuji, H., Okuno, T., Asahara, T., Nomoto, K., Shibata, A., Fujisawa, Y., Minato, T., Okamoto, A., et al. (2015). Intestinal dysbiosis and lowered serum lipopolysaccharide-binding protein in Parkinson's disease. PLoS ONE *10*, e0142164.

Hoban, A.E., Stilling, R.M., Ryan, F.J., Shanahan, F., Dinan, T.G., Claesson, M.J., Clarke, G., and Cryan, J.F. (2016). Regulation of prefrontal cortex myelination by the microbiota. Transl. Psychiatry *6*, e774.

Holmqvist, S., Chutna, O., Bousset, L., Aldrin-Kirk, P., Li, W., Björklund, T., Wang, Z.Y., Roybon, L., Melki, R., and Li, J.Y. (2014). Direct evidence of Parkinson pathology spread from the gastrointestinal tract to the brain in rats. Acta Neuropathol. *128*, 805–820.

Hooper, L.V., Littman, D.R., and Macpherson, A.J. (2012). Interactions between the microbiota and the immune system. Science *336*, 1268–1273.

Jenner, P. (2008). Molecular mechanisms of L-DOPA-induced dyskinesia. Nat. Rev. Neurosci. *9*, 665–677.

Jo, E., McLaurin, J., Yip, C.M., St George-Hyslop, P., and Fraser, P.E. (2000). alpha-Synuclein membrane interactions and lipid specificity. J. Biol. Chem. *275*, 34328–34334.

Kannarkat, G.T., Boss, J.M., and Tansey, M.G. (2013). The role of innate and adaptive immunity in Parkinson's disease. J. Parkinsons Dis. *3*, 493–514.

Keshavarzian, A., Green, S.J., Engen, P.A., Voigt, R.M., Naqib, A., Forsyth, C.B., Mutlu, E., and Shannon, K.M. (2015). Colonic bacterial composition in Parkinson's disease. Mov. Disord. *30*, 1351–1360.

Kim, C., Ho, D.H., Suk, J.E., You, S., Michael, S., Kang, J., Joong Lee, S., Masliah, E., Hwang, D., Lee, H.J., and Lee, S.J. (2013). Neuron-released oligomeric α-synuclein is an endogenous agonist of TLR2 for paracrine activation of microglia. Nat. Commun. *4*, 1562.

Klucken, J., Ingelsson, M., Shin, Y., Irizarry, M.C., Hedley-Whyte, E.T., Frosch, M., Growdon, J., McLean, P., and Hyman, B.T. (2006). Clinical and biochemical correlates of insoluble alpha-synuclein in dementia with Lewy bodies. Acta Neuropathol. *111*, 101–108.

Kohman, R.A., Bhattacharya, T.K., Kilby, C., Bucko, P., and Rhodes, J.S. (2013). Effects of minocycline on spatial learning, hippocampal neurogenesis and microglia in aged and adult mice. Behav. Brain Res. *242*, 17–24.

Kopylova, E., Noé, L., and Touzet, H. (2012). SortMeRNA: fast and accurate filtering of ribosomal RNAs in metatranscriptomic data. Bioinformatics *28*, 3211–3217.

Kumar, D.K., Choi, S.H., Washicosky, K.J., Eimer, W.A., Tucker, S., Ghofrani, J., Lefkowitz, A., McColl, G., Goldstein, L.E., Tanzi, R.E., and Moir, R.D. (2016). Amyloid-β peptide protects against microbial infection in mouse and worm models of Alzheimer's disease. Sci. Transl. Med. *8*, 340ra72.

Langille, M.G., Zaneveld, J., Caporaso, J.G., McDonald, D., Knights, D., Reyes, J.A., Clemente, J.C., Burkepile, D.E., Vega Thurber, R.L., Knight, R., et al. (2013). Predictive functional profiling of microbial communities using 16S rRNA marker gene sequences. Nat. Biotechnol. *31*, 814–821.

Ley, R.E., Peterson, D.A., and Gordon, J.I. (2006). Ecological and evolutionary forces shaping microbial diversity in the human intestine. Cell *124*, 837–848.

Lin, R., Jiang, Y., Zhao, X.Y., Guan, Y., Qian, W., Fu, X.C., Ren, H.Y., and Hou, X.H. (2014). Four types of Bifidobacteria trigger autophagy response in intestinal epithelial cells. J. Dig. Dis. *15*, 597–605.

Lozupone, C., and Knight, R. (2005). UniFrac: a new phylogenetic method for comparing microbial communities. Appl. Environ. Microbiol. *71*, 8228–8235.

Luk, K.C., Kehm, V., Carroll, J., Zhang, B., O'Brien, P., Trojanowski, J.Q., and Lee, V.M. (2012). Pathological α-synuclein transmission initiates Parkinson-like neurodegeneration in nontransgenic mice. Science *338*, 949–953.

Mandal, S., Van Treuren, W., White, R.A., Eggesbø, M., Knight, R., and Peddada, S.D. (2015). Analysis of composition of microbiomes: a novel method for studying microbial composition. Microb. Ecol. Health Dis. *26*, 27663.

Matcovitch-Natan, O., Winter, D.R., Giladi, A., Vargas Aguilar, S., Spinrad, A., Sarrazin, S., Ben-Yehuda, H., David, E., Zelada González, F., Perrin, P., et al. (2016). Microglia development follows a stepwise program to regulate brain homeostasis. Science *353*, aad8670.

Mayer, E.A., Padua, D., and Tillisch, K. (2014). Altered brain-gut axis in autism: comorbidity or causative mechanisms? BioEssays *36*, 933–939.

McDonald, D., Price, M.N., Goodrich, J., Nawrocki, E.P., DeSantis, T.Z., Probst, A., Andersen, G.L., Knight, R., and Hugenholtz, P. (2012). An improved Greengenes taxonomy with explicit ranks for ecological and evolutionary analyses of bacteria and archaea. ISME J. *6*, 610–618.

Minter, M.R., Zhang, C., Leone, V., Ringus, D.L., Zhang, X., Oyler-Castrillo, P., Musch, M.W., Liao, F., Ward, J.F., Holtzman, D.M., et al. (2016). Antibiotic-induced perturbations in gut microbial diversity influences neuro-inflammation and amyloidosis in a murine model of Alzheimer's disease. Sci. Rep. *6*, 30028.

Mitchell, R.W., On, N.H., Del Bigio, M.R., Miller, D.W., and Hatch, G.M. (2011). Fatty acid transport protein expression in human brain and potential role in fatty acid transport across human brain microvessel endothelial cells. J. Neurochem. *117*, 735–746.

Mogi, M., Harada, M., Kondo, T., Riederer, P., Inagaki, H., Minami, M., and Nagatsu, T. (1994a). Interleukin-1 beta, interleukin-6, epidermal growth factor and transforming growth factor-alpha are elevated in the brain from parkinsonian patients. Neurosci. Lett. *180*, 147–150.

Mogi, M., Harada, M., Riederer, P., Narabayashi, H., Fujita, K., and Nagatsu, T. (1994b). Tumor necrosis factor-alpha (TNF-alpha) increases both in the brain and in the cerebrospinal fluid from parkinsonian patients. Neurosci. Lett. *165*, 208–210.

Möhle, L., Mattei, D., Heimesaat, M.M., Bereswill, S., Fischer, A., Alutis, M., French, T., Hambardzumyan, D., Matzinger, P., Dunay, I.R., and Wolf, S.A. (2016). Ly6C(hi) monocytes provide a link between antibiotic-induced changes in gut microbiota and adult hippocampal neurogenesis. Cell Rep. *15*, 1945–1956.

Nalls, M.A., Pankratz, N., Lill, C.M., Do, C.B., Hernandez, D.G., Saad, M., DeStefano, A.L., Kara, E., Bras, J., Sharma, M., et al.; International Parkinson's Disease Genomics Consortium (IPDGC); Parkinson's Study Group (PSG) Parkinson's Research: The Organized GENetics Initiative (PROGENI); 23andMe; GenePD; NeuroGenetics Research Consortium (NGRC); Hussman Institute of Human Genomics (HIHG); Ashkenazi Jewish Dataset Investigator; Cohorts for Health and Aging Research in Genetic Epidemiology (CHARGE); North American Brain Expression Consortium (NABEC); United Kingdom Brain Expression Consortium (UKBEC); Greek Parkinson's Disease Consortium; Alzheimer Genetic Analysis Group (2014). Large-scale meta-analysis of genome-wide association data identifies six new risk loci for Parkinson's disease. Nat. Genet. *46*, 989–993.

Neufeld, K.M., Kang, N., Bienenstock, J., and Foster, J.A. (2011). Reduced anxiety-like behavior and central neurochemical change in germ-free mice. Neurogastroenterol. Motil. *23*, 255–264, e119.

Prusiner, S.B., Woerman, A.L., Mordes, D.A., Watts, J.C., Rampersaud, R., Berry, D.B., Patel, S., Oehler, A., Lowe, J.K., Kravitz, S.N., et al. (2015). Evidence for α-synuclein prions causing multiple system atrophy in humans with parkinsonism. Proc. Natl. Acad. Sci. USA *112*, E5308–E5317.

Ritz, B.R., Paul, K.C., and Bronstein, J.M. (2016). Of pesticides and men: a California story of genes and environment in Parkinson's disease. Curr. Environ. Health Rep. *3*, 40–52.

Rockenstein, E., Mallory, M., Hashimoto, M., Song, D., Shults, C.W., Lang, I., and Masliah, E. (2002). Differential neuropathological alterations in transgenic mice expressing alpha-synuclein from the platelet-derived growth factor and Thy-1 promoters. J. Neurosci. Res. *68*, 568–578.

Rooks, M.G., and Garrett, W.S. (2016). Gut microbiota, metabolites and host immunity. Nat. Rev. Immunol. *16*, 341–352.

Sacchettini, J.C., and Kelly, J.W. (2002). Therapeutic strategies for human amyloid diseases. Nat. Rev. Drug Discov. *1*, 267–275.

Sanchez-Guajardo, V., Barnum, C.J., Tansey, M.G., and Romero-Ramos, M. (2013). Neuroimmunological processes in Parkinson's disease and their relation to α-synuclein: microglia as the referee between neuronal processes and peripheral immunity. ASN Neuro *5*, 113–139.

Scheperjans, F., Aho, V., Pereira, P.A., Koskinen, K., Paulin, L., Pekkonen, E., Haapaniemi, E., Kaakkola, S., Eerola-Rautio, J., Pohja, M., et al. (2015). Gut microbiota are related to Parkinson's disease and clinical phenotype. Mov. Disord. *30*, 350–358.

Schroeder, B.O., and Bäckhed, F. (2016). Signals from the gut microbiota to distant organs in physiology and disease. Nat. Med. *22*, 1079–1089.

Selkrig, J., Wong, P., Zhang, X., and Pettersson, S. (2014). Metabolic tinkering by the gut microbiome: Implications for brain development and function. Gut Microbes *5*, 369–380.

Shannon, K.M., Keshavarzian, A., Dodiya, H.B., Jakate, S., and Kordower, J.H. (2012). Is alpha-synuclein in the colon a biomarker for premotor Parkinson's disease? Evidence from 3 cases. Mov. Disord. *27*, 716–719.

Sharon, G., Sampson, T.R., Geschwind, D.H., and Mazmanian, S.K. (2016). The central nervous system and the gut microbiome. Cell *167*, 915–932.

Smith, P.M., Howitt, M.R., Panikov, N., Michaud, M., Gallini, C.A., Bohlooly-Y, M., Glickman, J.N., and Garrett, W.S. (2013). The microbial metabolites, short-chain fatty acids, regulate colonic Treg cell homeostasis. Science *341*, 569–573.

Soldner, F., Stelzer, Y., Shivalila, C.S., Abraham, B.J., Latourelle, J.C., Barrasa, M.I., Goldmann, J., Myers, R.H., Young, R.A., and Jaenisch, R. (2016). Parkinson-associated risk variant in distal enhancer of α-synuclein modulates target gene expression. Nature *533*, 95–99.

Sudo, N., Chida, Y., Aiba, Y., Sonoda, J., Oyama, N., Yu, X.N., Kubo, C., and Koga, Y. (2004). Postnatal microbial colonization programs the hypothalamic-pituitary-adrenal system for stress response in mice. J. Physiol. *558*, 263–275.

Svensson, E., Horváth-Puhó, E., Thomsen, R.W., Djurhuus, J.C., Pedersen, L., Borghammer, P., and Sørensen, H.T. (2015). Vagotomy and subsequent risk of Parkinson's disease. Ann. Neurol. *78*, 522–529.

Unger, M.M., Spiegel, J., Dillmann, K.U., Grundmann, D., Philippeit, H., Bürmann, J., Faßbender, K., Schwiertz, A., and Schäfer, K.H. (2016). Short chain fatty acids and gut microbiota differ between patients with Parkinson's disease and age-matched controls. Parkinsonism Relat. Disord. *32*, 66–72.

Valera, E., and Masliah, E. (2016). Combination therapies: the next logical step for the treatment of synucleinopathies? Mov. Disord. *31*, 225–234.

Vázquez-Baeza, Y., Pirrung, M., Gonzalez, A., and Knight, R. (2013). EMPeror: a tool for visualizing high-throughput microbial community data. Gigascience *2*, 16.

Verbaan, D., Marinus, J., Visser, M., van Rooden, S.M., Stiggelbout, A.M., and van Hilten, J.J. (2007). Patient-reported autonomic symptoms in Parkinson disease. Neurology *69*, 333–341.

Wall, R., Cryan, J.F., Ross, R.P., Fitzgerald, G.F., Dinan, T.G., and Stanton, C. (2014). Bacterial neuroactive compounds produced by psychobiotics. Adv. Exp. Med. Biol. *817*, 221–239.

Walters, W., Hyde, E.R., Berg-Lyons, D., Ackermann, G., Humphrey, G., Parada, A., Gilbert, J.A., Jansson, J.K., Caporaso, J.G., Fuhrman, J.A., et al. (2015). Improved bacterial 16S rRNA gene (V4 and V4-5) and fungal internal transcribed spacer marker gene primers for microbial community surveys. mSystems *1*, 1.

Wang, L., Magen, I., Yuan, P.Q., Subramaniam, S.R., Richter, F., Chesselet, M.F., and Taché, Y. (2012). Mice overexpressing wild-type human alpha-synuclein display alterations in colonic myenteric ganglia and defecation. Neurogastroenterol. Motil. *24*, e425–e436.

Yano, J.M., Yu, K., Donaldson, G.P., Shastri, G.G., Ann, P., Ma, L., Nagler, C.R., Ismagilov, R.F., Mazmanian, S.K., and Hsiao, E.Y. (2015). Indigenous bacteria from the gut microbiota regulate host serotonin biosynthesis. Cell *161*, 264–276.

Zhang, J., Saur, T., Duke, A.N., Grant, S.G., Platt, D.M., Rowlett, J.K., Isacson, O., and Yao, W.D. (2014). Motor impairments, striatal degeneration, and altered dopamine-glutamate interplay in mice lacking PSD-95. J. Neurogenet. *28*, 98–111.

STAR★METHODS

KEY RESOURCES TABLE

REAGENT or RESOURCE	SOURCE	IDENTIFIER
Antibodies		
Anti-aggregated/fibril alpha-synuclein; MJFR-14-6-4-2	Abcam	Cat# ab209538
Anti-phospho Ser129 alpha-synuclein	BioLegend	Cat# 825701, RRID: AB_2564891
Anti-Iba1	Wako	Cat# 019-19741, RRID: AB_839504
Anti-mouse IgG-Alexafluor 488	Life Technologies	Cat# A-11001, RRID: AB_2534069
Anti-rabbit IgG-Alexafluor 546	Life Technologies	Cat# A-11010, RRID: AB_2534077
Neurotrace 435/455 Blue	Life Technologies	Cat# N-21479
Anti- alpha-synuclein	BD	Cat# 610787, RRID: AB_398108
Anti-mouse IgG-HRP	Cell Signaling Technology	Cat# 7076S
Anti-rabbit IgG-HRP	Cell Signaling Technology	Cat# 7074S
Chemicals, Peptides, and Recombinant Proteins		
Minocycline	Arcos / Fisher Scientific	Cat# AC455330010
Ampicillin	Sigma Aldrich	Cat# A0166
Vancomycin	Sagent Pharmaceuticals	Cat# 157-99
Neomycin	Fisher Scientific	Cat# BP26695
Gentamicin	Sigma Aldrich	Cat# G1264
Erythromycin	Sigma Aldrich	Cat# E5389
Sodium acetate	Sigma Aldrich	Cat# S5636
Sodium propionate	Sigma Aldrich	Cat# P5436
Sodium butyrate	Sigma Aldrich	Cat# 19364
Purified alpha synuclein	Abcam	Cat# ab51188
Thioflavin T	Sigma Aldrich	Cat# T3516
Critical Commercial Assays		
Alpha-synuclein ELISA	ThermoFisher	Cat# KHB0061
iScript cDNA Synthesis kit	Biorad	Cat# 170-8890
SyberGreen qPCR Master Mix	Applied Biosystems	Cat# 4309155
IL-6 ELISA	eBioscience	Cat# 88-7324
TNF ELISA	eBioscience	Cat# 88-7064
MoBio Power Soil Kit	MoBio Laboratories	Cat# 12888-50
Deposited Data		
16 s RNA sequences	QIITA; https://qiita.ucsd.edu/	10483
16 s RNA sequences	EMBL, ENA; http://www.ebi.ac.uk/ena	ERP019564
Experimental Models: Organisms/Strains		
Mouse: Thy1-alpha synuclein	Marie Francoise-Chesselet, University of California, Los Angeles	N/A
Mouse: BDF1	Generated from B6 x DBA	N/A
Mouse: C57BL/6	Charles River	Strain: 027
Mouse: DBA/2	Charles River	Strain: 026
Bacteria: *Escherichia coli* K12 MC4100	Matt Chapman, University of Michigan	N/A
Sequence-Based Reagents		
Primers: *hu-snca* - Fwd: 5′-TTGCAGCAGCCACTGGCT TTG-3′ and Rev: 5′-GGATCCACAGGCATATCTTCCAGAA-3′	PrimerBank	N/A
Primers: *tnfa*- Fwd: 5′-CCCTCACACTCAGATCATCTTCT-3’ and Rev: 5′-GCTACGACGTGGGCTACAG-3′	PrimerBank	N/A

(*Continued on next page*)

Continued

REAGENT or RESOURCE	SOURCE	IDENTIFIER
Primers: *il6* – Fwd: 5′-TAGTCCTTCCTACCCCAATTTCC-3′ and Rev: 5′-TTGGTCCTTAGCCACTCCTTC-3′	PrimerBank	N/A
Primers: *ddit4* - Fwd: 5′-CAAGGCAAGAGCTGCCATAG-3′ and Rev: 5′-CCGGTACTTAGCGTCAGGG-3′	PrimerBank	N/A
Primers: *bdnf* - Fwd: 5′-TCATACTTCGGTTGCATGAAGG-3′ and Rev:5′-AGACCTCTCGAACCTGCCC-3′	PrimerBank	N/A
Primers: *gapdh* - Fwd: 5′-CATGGCCTTCCGTGTTCCTA-3′ and Rev: 5′-CCTGCTTCACCACCTTCTTGAT-3′	PrimerBank	N/A
Software and Algorithms		
ImageJ	National Institutes of Health	https://imagej.nih.gov/ij/
Imaris	Bitplane	http://www.bitplane.com/imaris/imaris
SortMeRNA 2.0	Kopylova et al. (2012)	http://bioinfo.lifl.fr/RNA/sortmerna/
Greengenes	Lawrence Berkeley National Labs	http://greengenes.lbl.gov/cgi-bin/nph-index.cgi
QIIME 1.9	Rob Knight laboratory, UCSD and Greg Caporaso laboratory, Northern Arizona University	http://qiime.org/
Seaborn 0.70	Michael Waskom, Stanford University	http://seaborn.pydata.org/

CONTACT FOR REAGENT AND RESOURCE SHARING

As Lead Contact, Sarkis K. Mazmanian (California Institute of Technology) is responsible for all reagent and resource requests. Please contact Sarkis K. Mazmanian at sarkis@caltech.edu with requests and inquiries.

EXPERIMENTAL MODEL AND SUBJECT DETAILS

Mice

Female BDF1 background, Thy1-αSyn animals heterozygous for the Thy1-α-synuclein transgene on the X chromosome were bred with wild-type male BDF1 mice to generate the male ASO and WT littermates used in the study (Chesselet et al., 2012; Rockenstein et al., 2002). Male BDF1 were bred by crossing female C57BL/6 with DBA/2 males (Charles River, Hollister, CA). Breeding pairs were replenished every 6 months with transgenic females and newly generated BDF1 males. Germ-free (GF) Thy1-αSyn breeding pairs were generated via caesarian section and males newly generated every 6 months. Following surgical removal of the uterus and delivery of pups, microbiologically-sterile animals were fostered by GF Swiss-Webster dams. SPF, antibiotic-treated, and ex-GF animals were housed in autoclaved, ventilated, microisolator caging. GF and SCFA-treated animals were housed in open-top caging within flexible film isolators and maintained microbiologically sterile. Microbial sterility was confirmed on a bi-weekly basis through 16 s rRNA PCR from fecal-derived DNA and plating of fecal pellets on Brucella blood agar media under anaerobic conditions and tryptic soy blood agar under aerobic conditions. All animals, irrespective of colonization status, received autoclaved food (LabDiet Laboratory Autoclavable Diet 5010, St Louis, MO) and water ad libitum, were maintained on the same 12 hr light-dark cycle, and housed in the same facility. Antibiotic-treated animals were provided ampicillin (1g/L; Sigma Aldrich, St. Louis, MO), vancomycin (0.5g/L; Sagent Pharmaceuticals, Schaumburg, IL), neomycin (0.5g/L; Fisher Scientific), gentamycin (100mg/L; Sigma Aldrich), and erythromycin (10mg/L; Sigma Aldrich) in drinking water beginning at 5-6 weeks of age through 12-13 weeks of age. Ex-GF animals were generated by colonizing 5-6 week old GF animals with cecal contents from 3 wild-type BDF1 males resuspended in sodium bicarbonate buffer prior to oral gavage. SCFA treated animals were provided with drinking containing sodium acetate (67.5mM; Sigma Aldrich), sodium propionate (25mM; Sigma Aldrich), and sodium butyrate (40mM; Sigma Aldrich) beginning at 5-6 weeks of age until 12-13 weeks of age (Smith et al., 2013). Minocycline (Arcos Organics) treatment was provided in drinking water ad libitum at 2g/L, concurrently with SCFAs from 5-6 weeks of age until 12-13 weeks (Kohman et al., 2013). GF animals treated with heat-killed bacteria were provided ~$5x10^8$ cfu/mL of lysogeny broth (LB)-grown *Escherichia coli* MC4100 (a kind gift from Matthew Chapman, U. of Michigan), washed twice in phosphate buffered saline and boiled for 45min, in drinking water ad libitum. All animal husbandry and experiments were approved by the California Institute of Technology's Institutional Animal Care and Use Committee (IACUC).

Human Donor and Criteria

Human donors were selected from patients seen at the Movement Disorder Clinic at Rush University. PD was diagnosed according to the UK Brain Bank Criteria. Exclusion criteria for PD subjects: atypical or secondary Parkinsonism; the use of probiotics or antibiotics

within three months prior to sample collection; use of NSAIDs; primary gastrointestinal pathology; history of chronic GI illness (including IBD and celiac disease); unstable medical, neurological, or psychiatric illness; low platelet count (< 80k); uncorrectable prolonged PT 9 > 15sec); or history of bleeding that precludes biopsies. All patients had normal mucosa in their rectum and sigmoid by sigmoidoscopy and by H&E histology. Healthy controls were matched as closely as possible to PD patients. Inclusion criteria for healthy subjects: normal physical exam and blood work; no digestive complaints, symptoms, or history of disease; no neurodegenerative disease; no probiotic, antibiotic, NSAIDs, or prescription medication use at least three months prior to sample collection. All human studies were approved under both Rush University and California Institute of Technology Institutional Review Board (IRB).

METHOD DETAILS

Motor Function and Gastrointestinal Testing

Excluding humanized animals, all motor function assessment was performed in the identical, gnotobiotic animal facility. Humanized animals were tested within a laminar-flow biosafety cabinet in the same facility. Motor function for all animals was tested between hours 7 and 9 of the light-phase. All tests were performed similarly to previous studies (Fleming et al., 2004). Beam traversal was performed first, before allowing animals to rest for ~1hr and testing on pole descent. The following day, adhesive removal and hindlimb scoring was performed. Fecal output was performed within 3 days and immediately prior to tissue collection.

Beam Traversal

A 1 m plexiglass beam (Stark's Plastics, Forest Park, OH) was constructed of four segments of 0.25 m in length. Each segment was of thinner widths 3.5cm, 2.5cm, 1.5cm, and 0.5cm, with 1cm overhangs placed 1cm below the surface of the beam. The widest segment acted as a loading platform for the animals and the narrowest end placed into home cage. Animals had two days of training to traverse the length of the beam before testing. On the first day of training, animals received 1 trial with the home cage positioned close to the loading platform and guided the animals forward along the narrowing beam. Animals received two more trials with limited or no assistance to encourage forward movement and stability on the beam. On the second day of training, animals had three trials to traverse the beam and generally did not require assistance in forward movement. On the third day, animals were timed over three trials to traverse from the loading platform and to the home cage. Timing began when the animals placed their forelimbs onto the 2.5cm segment and ended when one forelimb reached the home cage.

Pole Descent

A 0.5 m long pole, 1cm in diameter, wrapped with non-adhesive shelf liner to facilitate the animals grip, was placed into the home cage. Animals received two days of training to descend from the top of the pole and into the home cage. On day one of training, animals received 3 trials. The first trial, animals were placed head-down 1/3 the distance above the floor, the second trial from 2/3 the distance, and the third trial animals were placed at the top. The second day of training, animals were given 3 trials to descend, head-down, from the top of the pole. On the test day, animals were placed head-down on the top of the pole and timed to descend back into the home cage. Timing began when the experimenter released the animal and ended when one hind-limb reached the home cage base.

Adhesive Removal

¼" round adhesive labels (Avery, Glendale, CA) were placed on the nasal bridge between the nostrils and forehead. Animals were placed into their home cage (with cage mates removed) and timed to completely remove the sticker. Animals were recorded over three trials.

Hindlimb Clasping Reflex Scoring

Animals were gently lifted upward by the mid-section of the tail and observed over ~5-10 s (Zhang et al., 2014). Animals were assigned a score of 0, 1, 2, 3 based on the extent to which the hindlimbs clasped inward. 0, indicating no clasping, was given to animals that freely moved both their limbs and extended them outward. A score of 1 was assigned to animals which clasped one hindlimb inward for the duration of the restraint or if both legs exhibited partial inward clasping. A score of 2 was given if both legs clasped inward for the majority of the observation, but still exhibited some flexibility. A score of 3 was assigned if animals displayed complete paralysis of hindlimbs that immediately clasped inward and exhibited no signs of flexibility.

Inverted Grid

Animals were placed in the center of a 30cm by 30cm screen with 1cm wide mesh. The screen was inverted head-over-tail and placed on supports ~40cm above an open cage with deep bedding. Animals were timed until they released their grip or remained for 60 s.

Fecal Output

Animals were removed from their home cages and placed into a 12cm x 25cm translucent cylinder. Fecal pellets were counted every 5 min, cumulative over 15 min. Principal component analysis of all motor function was performed using MATLAB software (MathWorks) using behavioral data collected from subjects that performed at least 3 tasks. Data was centered and standardized ($\sigma = 1$) prior to running the pca function. Only PC1 and PC2, which accounted for 70.5% of the variance, were plotted using the corresponding factor loadings for each individual subject.

Immunostaining and Microglia Reconstructions

Animals were sedated with pentobarbital and well-perfused with phosphate-buffered saline, brains were dissected and hemispheres fixed in 4%(w/v) paraformaldehyde. 50 μm sagittal sections were generated via vibratome. Free-floating sections were stained with anti-aggregated/fibril αSyn MJFR1 (1:1000; rabbit; AbCam, Cambridge UK), anti-phosphoSer129 αSyn (1:1000; mouse; Biolegend, San Diego, CA), and Neurotrace (Life Technologies, Carlsbad, CA), or with anti-Iba1 (1:1000; rabbit; Wako, Richmond, VA) and subsequently stained with anti-mouse IgG-AF488 and anti-rabbit IgG-AF546 (1:1000; Life Technologies). Sections were mounted with ProFade Diamond (Life Technologies), and imaged with a 10X objective on a Zeiss LSM800 confocal microscope. 2-3 fields per region per animal were imaged and compiled in ImageJ software for analysis. For microglia reconstructions, z stacks were imaged at 1 μm steps and subsequently analyzed using Imaris software, as previously described (Erny et al., 2015). Semi-automated reconstruction of microglia cell bodies and processes were performed, whereby the experimenter designates individual cell bodies and the software quantifies diameter, dendrite length, and branch points from each given cell body. 20-60 cells per region per animal were analyzed.

CD11b Enrichment and qPCR Analysis

Perfused whole brains were homogenized in PBS via passage through a 100 μm mesh filter, myelin debris were removed using magnetic separation with Myelin Removal Beads (Miltenyi Biotec, San Diego CA), according to manufacturer's instructions. CD11b enrichment was performed similarly, with magnetic enrichment by Microglia Microbeads (Miltenyi Biotec), according to manufacturer's instructions. Generally, greater than 90% of cells enriched stained positive for CD11b by immunofluorescence microscopy. For RNA analysis, dissected tissue (frontal cortex, caudoputamen, inferior midbrain, and cerebellum) or CD11b-enriched cell pellets, were lysed in Trizol for DirectZol RNA extraction (Zymo Research, Irvine, CA). cDNA was generated via iScript cDNAsynthesis kit (BioRad, Hercules, CA). qRT-PCR was performed with SybrGreen master mix (Applied Biosystems, Foster City, CA) on an AB 7900ht instrument using primers derived from PrimerBank for the indicated target genes and quantified as $\Delta\Delta C_T$, relative to *gapdh* (Primers listed in associated Resource Table).

Cytokine and αSyn ELISAs and Western Blots

Tissue homogenates were prepared in RIPA buffer containing protease inhibitor cocktail (ThermoFisher, Pittsburgh, PA) and diluted into PBS. TNF-α and IL-6 ELISAs (eBioscience, San Diego, CA) and αSyn ELISAs (ThermoFisher) were performed according to manufacturer's instructions. For dot blot quantification of αSyn fibrils, 1 μg of tissue homogenate from the specified region was spotted in 1 μL volume aloquats onto 0.45 μm nitrocellulose membranes. For Triton X- soluble versus insoluble fraction western blots, brain hemispheres were homogenized in RIPA buffer containing 1% Triton X-100, centrifuged at 15k x *g* for 60 min at 4°C to precipitate insoluble proteins from the Triton soluble supernatant. The insoluble fraction was solubilized in 10% sodium dodecyl sulfate, as previously described (Klucken et al., 2006). 5 μg of each fraction was separated by 4%–20% SDS-PAGE (ThermoFisher), blotted onto PVDF membranes. All membranes were blocked with 5% dry skim milk in Tris-buffered saline with 0.1% Tween-20. Anti-aggregated αSyn antibody (1:2000; rabbit; Abcam) or anti-αSyn (1:1000; mouse; BD) was diluted in skim milk and incubated overnight at 4°C. Membranes were probed with anti-rabbit or anti-mouse IgG HRP (1:1000; Cell Signaling Technology). All blots were detected with the Clarity chemiluminescence substrate (BioRad) on a BioRad GelDoc XR. Densitometry was performed using ImageJ software.

αSyn Aggregation Assays

For in vitro aggregation kinetics, 70 μM αSyn was purified as described previously (Chorell et al., 2015), and incubated in phosphate-buffered saline solution (0.01 M phosphate buffer, 0.0027 M potassium chloride, 0.137M sodium chloride, pH 7.4) in the presence of 12 μM of Thioflavin T (ThT; Sigma Aldrich) and increasing concentrations of SCFA. A nonbinding 96-well plate with half area (Corning #3881) was used for each experiment and a 2 mm diameter glass bead was added to each well to accelerate the aggregation. The ThT fluorescence signal was recorded using a microplate reader (Fluostar OPTIMA Microplate reader, BMG Labtech) with the excitation filter of 440 ± 10nm and an emission filter of 490 ± 10nm under intermittent shaking conditions at 37°C. The kinetic curves were normalized to the fluorescence maxima and the time to reach half-maximum intensity quantified. For atomic force microscopy (AFM) imaging, samples were diluted with ultrapure water to ~3 μM total protein concentration, and 50 μls were pipetted onto freshly cleaved mica and left to dry. The samples were imaged with a Modular scanning probe microscope NTEGRA Prima (NT-MDT) in intermittent contact mode in air using a gold-coated single crystal silicon cantilever (spring constant of ~5.1 N/m) with a resonance frequency of ~150 kHz. AFM images were processed with Gwyddion open source software.

SCFA Extraction and Analysis

Fecal samples were collected from animals at 12 weeks of age. Each fecal pellet was mixed with 1mL sterile 18 Ω de-ionized water. The pellet-water mixtures were homogenized by mixing at 3200 rpm for five minutes and centrifuged for 15 min at 13,000 rpm at 4°C. Supernatants were filtered using Acrodisc LC 13 mm sterile syringe filters with 0.2 μm PVDF membranes (Pall Life Sciences). The filtrates were used for high performance liquid chromatography (HPLC) analysis. Short chain fatty acids (SCFAs) were analyzed using HPLC (LC-20AT, Shimadzu) equipped with a carbohydrate column (Aminex HPX-87H column, Biorad) and photodiode array detector (PDA, Shimadzu). The eluent was 5 mM H_2SO_4, fed at a flowrate of 0.6 mL/min, and the column temperature was 50°C. The run time

was 60 min. Standard curves were generated by diluting 10 mM volatile fatty acid standard solution (acetic acid, butyric acid, formic acid, valeric acid, isovaleric acid, caproic acid, isocaproic acid, and heptanoic acid) to 50 nM to 5000 nM. Concentrations of SCFAs were normalized to soluble chemical oxygen demand. sCOD values of the fecal supernatants were measured with high range (20-1500 mg/L) Hach COD digestion tubes (Hach Company, Loveland) as recommended by the manufacturer. The wavelength used to measure COD with Hach spectrophotometer was 620 nm.

Microbiome Profiling

Fecal pellets were collected at day 7, 14, 21, and 49 post fecal transplant, from animals housed in groups of 1-3 by genotype and donor. Samples were sequenced according to the Earth Microbiome Project protocols (Gilbert et al., 2014). Briefly, DNA was extracted using a MoBio Power soil kit (Carlsbad, CA), and the V4 region of the 16S rRNA gene was amplified using barcoded primers (Walters et al., 2015). Sequencing was performed using an Illumina MiSeq. Operational Taxonomic Units (OTUs) were picked closed reference using SortMeRNA 2.0 (Kopylova et al., 2012) against the August 2013 release of Greengenes (McDonald et al., 2012) in QIIME 1.9 (Caporaso et al., 2010). The table was rarefied to 7500 sequences per sample for alpha and beta diversity calculations. Differential abundance was performed on a table filtered to exclude samples with less than 7500 sequences. Weighted and unweighted UniFrac (Lozupone and Knight, 2005) distances were calculated in QIIME 1.9. Principle Coordinate Analysis (PCoA) projections were visualized using Emperor 0.9.4 (Vázquez-Baeza et al., 2013). Function was inferred using PICRUSt 1.0 (Langille et al., 2013); predicted functional repertoires were compared using Bray Curtis distance. Significance tests were performed using permanova in scikit-bio 0.4.2 and permutative t tests in QIIME 1.9, both with 999 permutations per test. Differential abundance calculations were performed using genus-level taxa and KEGG-based relative abundance of all counts offset by one. Tests were performed using ANCOM (Mandal et al., 2015) in scikit-bio 0.4.2 with a one-way ANOVA test with a Bonferroni-corrected alpha of 0.1 as the rejection threshold. Mice colonized with samples from healthy donors or donors with PD were compared in the BDF1 or Thy1-αSyn genetic backgrounds. Significantly different taxa were compared between the groups, and classified as significant in both, significant in the Thy1-αSyn background only, or significant in the BDF1 background. Plots were generated using Seaborn 0.7.0.

QUANTIFICATION AND STATISTICAL ANALYSIS

Microbiome population statistics are described in detail above. Excluding these, datasets were analyzed within GraphPad Prism 6 software. Pairwise comparisons were generated with two-tailed t tests. Comparisons of groups were generated with one-way ANOVA. *P* –values, *n* values, definition of center and dispersion measurements are indicated in the associated figure legends for each figure.

DATA AND SOFTWARE AVAILABILITY

16 s sequencing data and metadata are available online through the QIITA website (https://qiita.ucsd.edu/) with the study accession #10483 and the EMBL ENA database (http://www.ebi.ac.uk/ena) with the study accession # ERP019564.

Cell

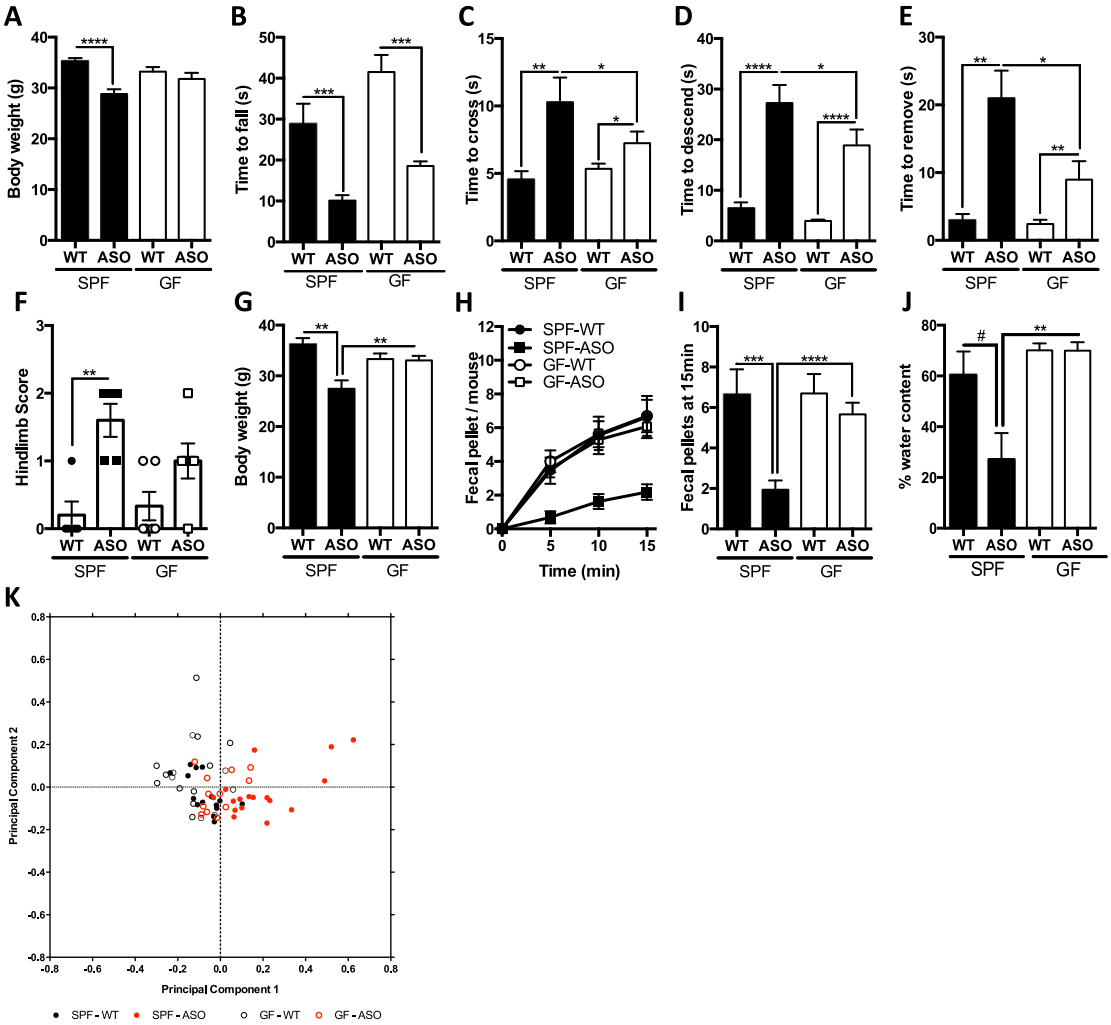

Figure S1. Body Weight of SPF and GF Animals, and Analysis of Aged Mice, Related to Figure 1

(A) Body weight of 12-13 week old animals.
(B) Time to fall from inverted grid by 12-13 week old animals.
(C) Time to traverse beam by 24-25 week old animals.
(D) Time to descend pole by 24-25 week old animals.
(E) Time to removal adhesive from nasal bridge by 24-25 week old animals.
(F) Hindlimb clasping reflex scores by 24-25 week old animals.
(G) Body weight of 24-25 week old animals.
(H) Time course of fecal output in a novel environment over 15 min by 24-25 week old animals.
(I) Total fecal pellets produced in 15 min by 24-25 week old animals.
(J) Percent water content in fecal pellets from 12-13 week old animals.
(K) Principle Component Analysis compiling all motor function scores from SPF-WT, SPF-ASO, GF-WT, and GF-ASO cohorts.
N = 4-6, error bars represent the mean and standard error. From 3 trials per animal for motor tests. Data are representative of 2 experiments. $^{\#}0.1 > p > 0.05$; $^{*}p \leq 0.05$; $^{**}p \leq 0.01$; $^{***}p \leq 0.001$; $^{****}p \leq 0.0001$. SPF = specific-pathogen free, GF = germ-free, WT = wild-type, ASO = Thy1-α-synuclein genotype.

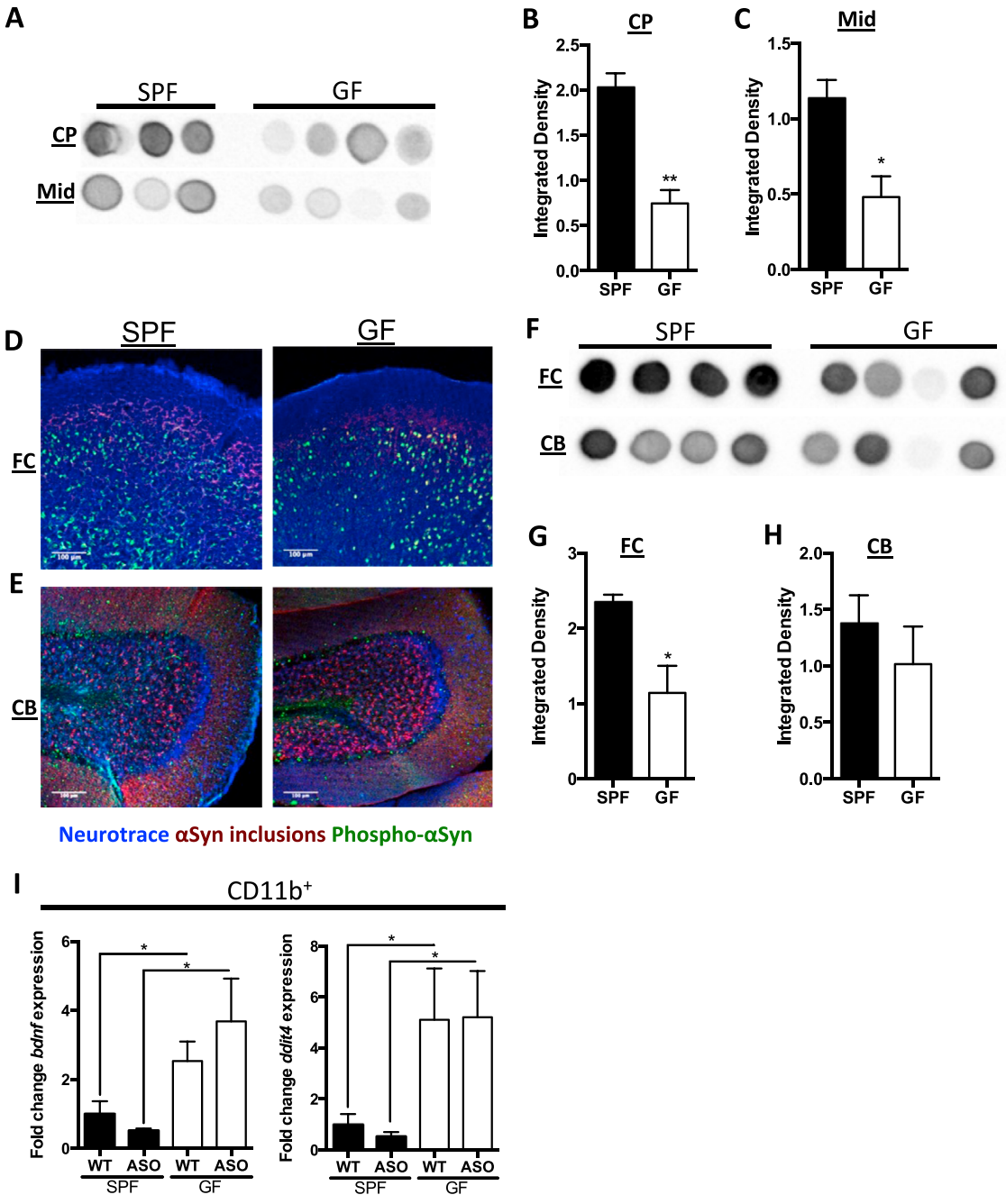

Figure S2. Gut Microbes Promote Regional-Specific αSyn Pathology, Related to Figures 2 and 3

(A) Aggregate-specific αSyn dot blots derived from caudoputamen (CP) and inferior midbrain (Mid) homogenates from SPF-ASO and GF-ASO animals.

(B and C) Densitometry quantification of dot blots of the (B) CP or (C) inferior midbrain.

(D) Representative images of the frontal cortex (FC) from SPF-ASO or GF-ASO animals stained with aggregation-specific αSyn antibody (red), Phospho-Ser129-αSyn antibody (green), and Neurotrace/Nissl (blue).

(E) Representative images of the cerebellum (CB) from SPF-ASO or GF-ASO animals, stained as above.

(F) Dot blot images of homogenates from the FC or CB from SPF-ASO and GF-ASO animals, immunostained with aggregation-specific αSyn antibody.

(G and H) Densitometry quantification of dot blots from the (G) FC and (H) CB.

(I) qPCR analysis of $CD11b^+$ cells derived from brain homogenate for *bdnf* and *ddit4*.

Animals were tested at 12-13 weeks of age. N = 3-4, error bars represent the mean and standard error. *$p \leq 0.05$. SPF = specific pathogen free, GF = germ-free, WT = wild-type, ASO = Thy1-α-synuclein genotype.

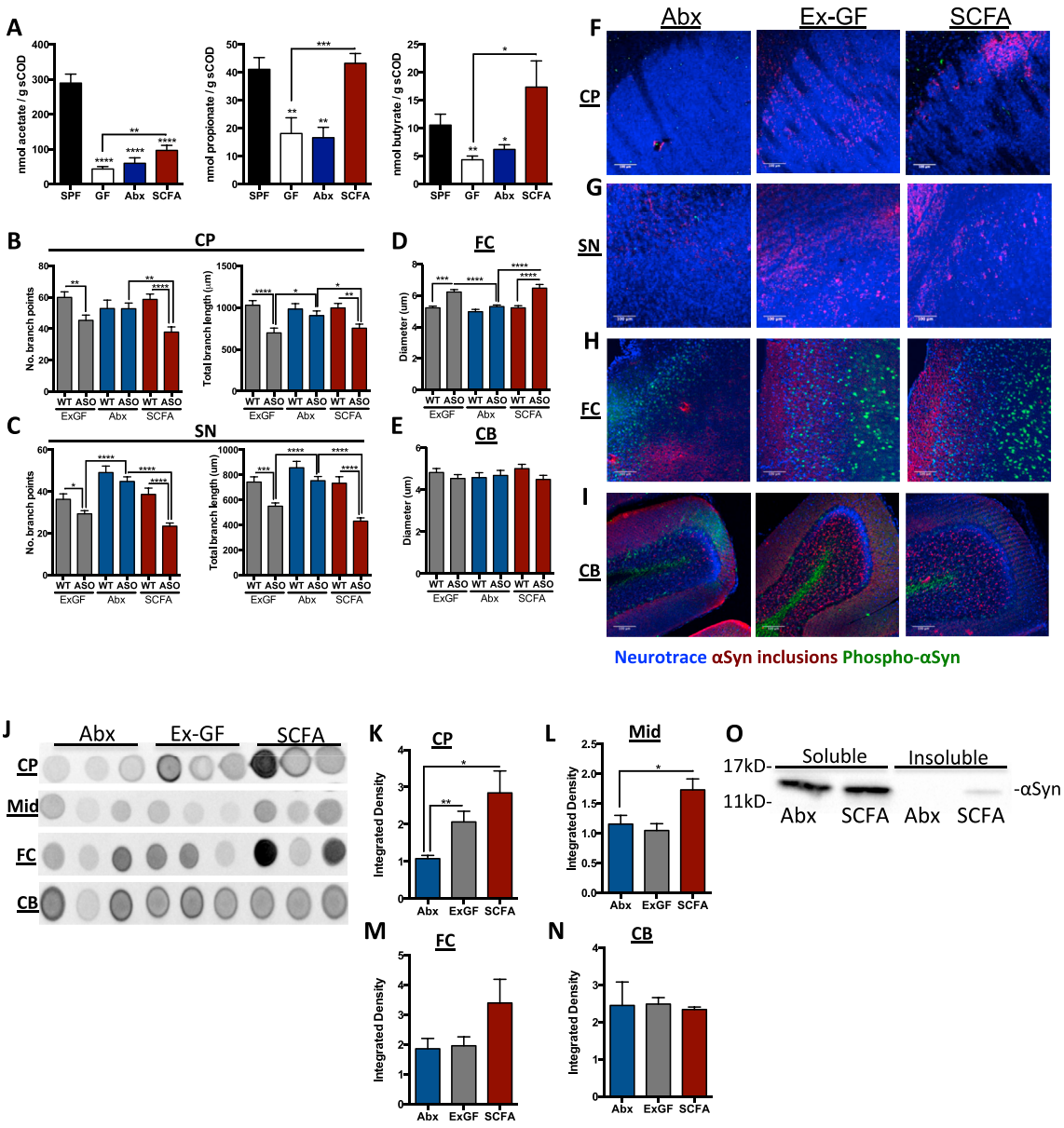

Figure S3. SCFA Alterations and Increased αSyn Pathology in Abx, Ex-GF, and SCFA Mice, Related to Figures 4 and 5

(A) Fecal concentrations of acetate, propionate, and butyrate, normalized by soluble chemical oxygen demand (sCOD).

(B) Caudoputamen (CP) -resident microglia parameters: number of branch points and total branch length.

(C) Substantia nigra (SN)-resident microglia parameters: number of branch points and total branch length.

(D and E) Diameter of microglia resident in the (D) frontal cortex (FC) and (E) cerebellum (CB).

(F–I) Representative images of the (F) CP, (G) SN, (H) FC, and (I) CB from Abx-ASO, ex-GF-ASO, or SCFA-ASO animals stained with aggregation-specific αSyn antibody (red), Phospho-Ser129-αSyn antibody (green), and Neurotrace/Nissl (blue).

(J) Dot blot images of CP, inferior midbrain (Mid), FC, and CB homogenate from Abx-ASO, ex-GF-ASO, and SCFA-ASO animals immunostained with aggregation-specific αSyn antibody.

(K–N) Densitometry quantification of dot blots from the (K) CP, (L) inferior midbrain, (M) FC, and (N) CB.

(O) Western blot for αSyn from Triton soluble and insoluble fractions of CP homogenates derived from Abx- and SCFA-ASO animals.

Animals were tested at 12-13 weeks of age. N = 3-6, with 20-60 microglia per region analyzed. Error bars represent the mean and standard error. *$p \leq 0.05$; **$p \leq 0.01$; ***$p \leq 0.001$; ****$p \leq 0.0001$. SPF = specific pathogen free, GF = germ-free, Abx = antibiotic-treated animals, Ex-GF = recolonized germ-free animals, SCFA = short-chain fatty acid-treated animals, WT = wild-type, ASO = Thy1-α-synuclein genotype.

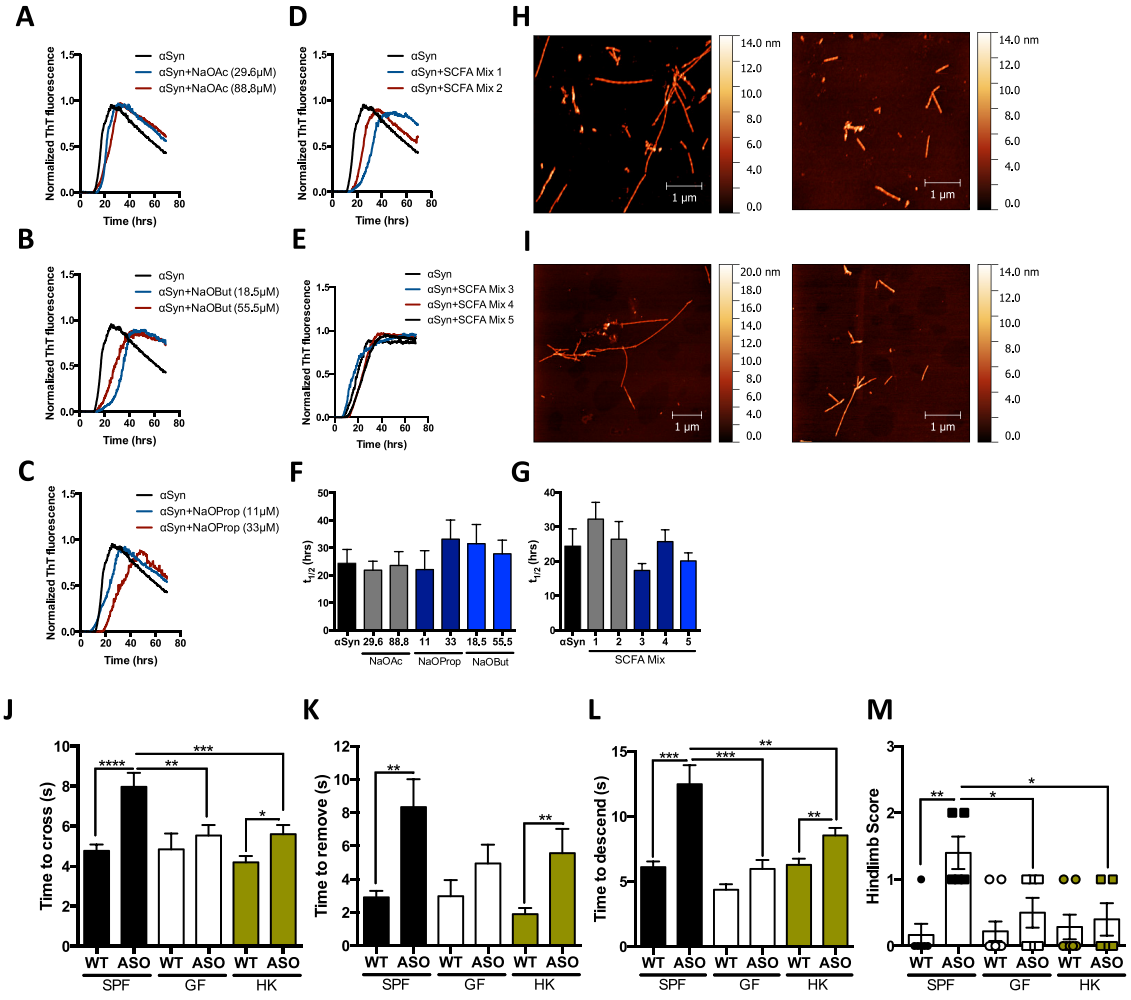

Figure S4. SCFAs Do Not Directly Alter αSyn Aggregation, Related to Figure 5

(A–C) αSyn aggregation kinetics, as measured by ThT fluorescence in the presence of the indicated concentrations of (A) sodium acetate, (B) sodium propionate, or (C) sodium butyrate.

(D and E) αSyn aggregation kinetics, as measured by ThT fluorescence in the presence of independent mixtures of SCFAs. (D) SCFA Mix 1- 29.6 μM acetate, 11 μM propionate, and 18.5 μM butyrate; SCFA Mix 2- 88.8 μM acetate, 33 μM propionate, and 55.5 μM butyrate. (E) SCFA Mix 3- 0.4 mM acetate, 0.15 mM propionate, and 0.24 mM butyrate; SCFA Mix 4-0.8 mM acetate, 0.3 mM propionate, and 0.47 mM butyrate; SCFA Mix 5- 2.0 mM acetate, 0.74 mM propionate, and 1.18 mM butyrate.

(F and G) Time to half-max fluorescence intensity for (F) individual SCFA treatments or (G) SCFA mixtures. N = 3, bars represent the mean and standard error.

(H and I) Representative atomic force microscopy of the final product from the above αSyn aggregation assays in the (H) absence of SCFA or (I) presence of SCFA Mix 1.

(J) Time to cross beam.

(K) Time to descend pole.

(L) Time to remove nasal adhesive.

(M) Hindlimb reflex scores.

Animals were tested at 12-13 weeks of age. N = 6-12, error bars represent the mean and standard error from 3 trials per animal. Data are compiled from 2 independent cohorts and plotted with controls from Figure 4 for clarity. *p ≤ 0.05; **p ≤ 0.01; ***p ≤ 0.001; ****p ≤ 0.0001. SPF = specific pathogen free; GF = germ-free; HK = heat-killed bacteria-treated; WT = wild-type, ASO = Thy1-α-synuclein genotype.

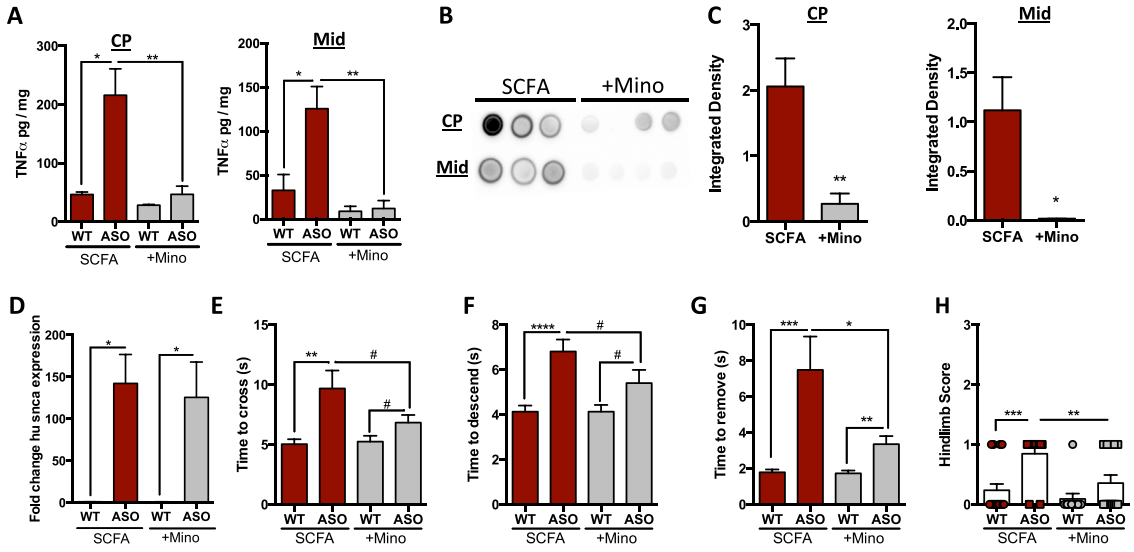

Figure S5. Minocycline Reduces SCFA-Induced αSyn Motor Deficits and Pathology, Related to Figure 5

(A) ELISA analysis for TNFα present in the caudoputamen (CP) and inferior midbrain (Mid).

(B) Dot blot images of CP, inferior midbrain (Mid) homogenates for aggregate-specific αSyn.

(C) Densitometry quantification of dot blots from the CP and inferior midbrain (Mid).

(D) qPCR analysis for human *snca* expression in total brain homogenate.

(E) Time to traverse beam apparatus.

(F) Time to descend pole.

(G) Time to remove nasal adhesive.

(H) Hindlimb clasping reflex score.

Animals were tested at 12-13 weeks of age. N = 6-12, error bars represent the mean and standard error from 3 trials per animal. Data are compiled from 2 independent cohorts. $^{\#}0.05 < p < 0.1$; $^{*}p \leq 0.05$; $^{**}p \leq 0.01$; $^{***}p \leq 0.001$; $^{****}p \leq 0.0001$. SPF = specific pathogen free; GF = germ-free; WT = wild-type, ASO = Thy1-α-synuclein genotype.

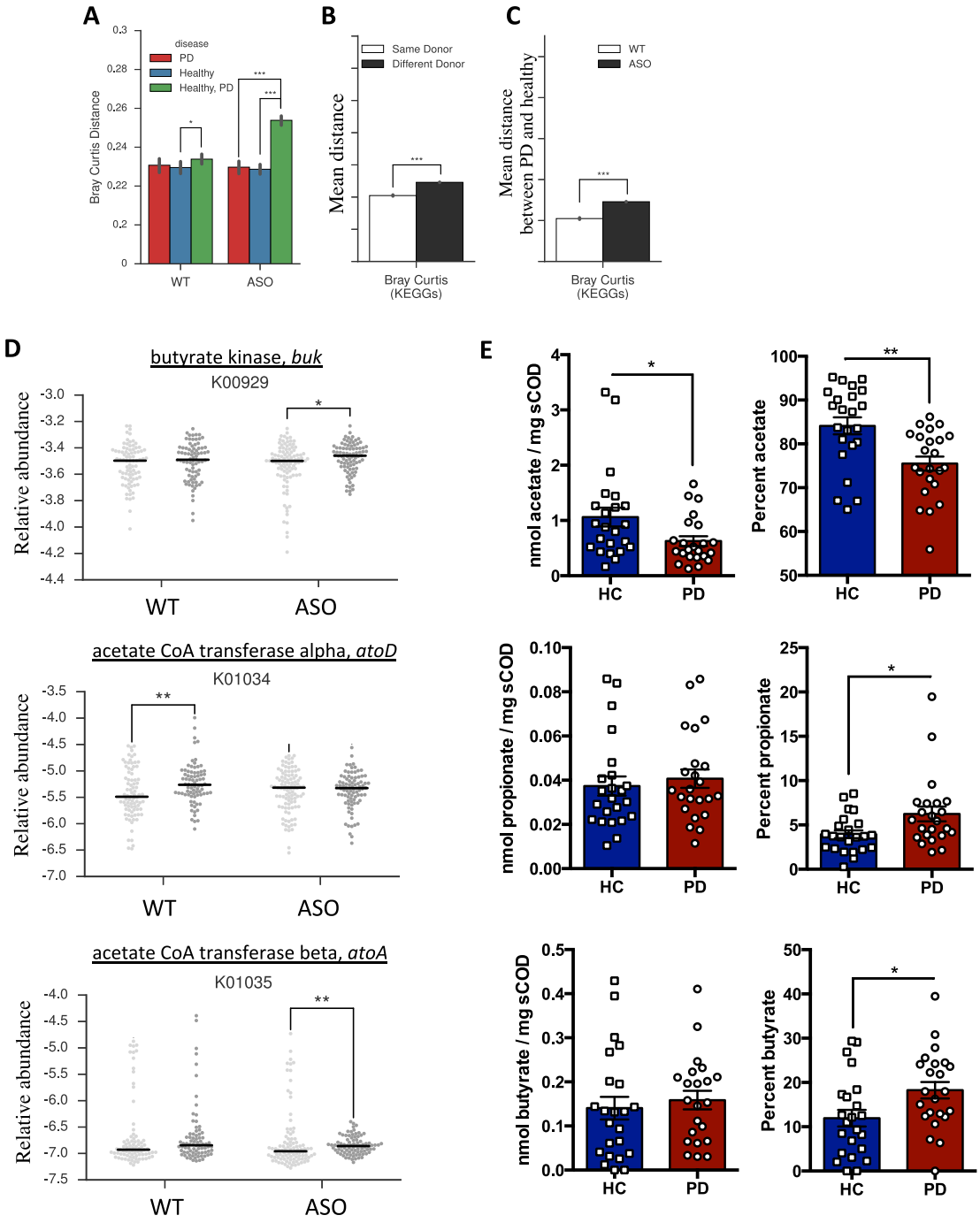

Figure S6. Microbial Metabolic Pathways Are Altered in Humanized Animals, Related to Figure 6

(A) Bray-Curtis distance comparisons between humanized groups.

(B and C) Bray-Curtis mean distance comparisons between (B) identical versus different donors, or (C) wild-type (WT) versus Thy1- α-synuclein (ASO) genotypes.

(D) PICRUSt analysis for specific KEGG families involved in SCFA production, light circles = healthy control derived microbes, dark circles = PD derived microbes.

(E) Fecal concentrations and relative abundances of acetate, propionate, and butyrate from humanized animals, normalized to soluble chemical oxygen demans. Compiled from 6 independent donor pairs, HC = healthy controls; PD = Parkinson's disease.

N = 3-6, over 3 time points post-colonization for KEGG analysis, N = 21-24 for SCFA abundances. Error bars represent the mean and standard error. *$p \leq 0.05$; **$p \leq 0.01$; ***$p \leq 0.001$.

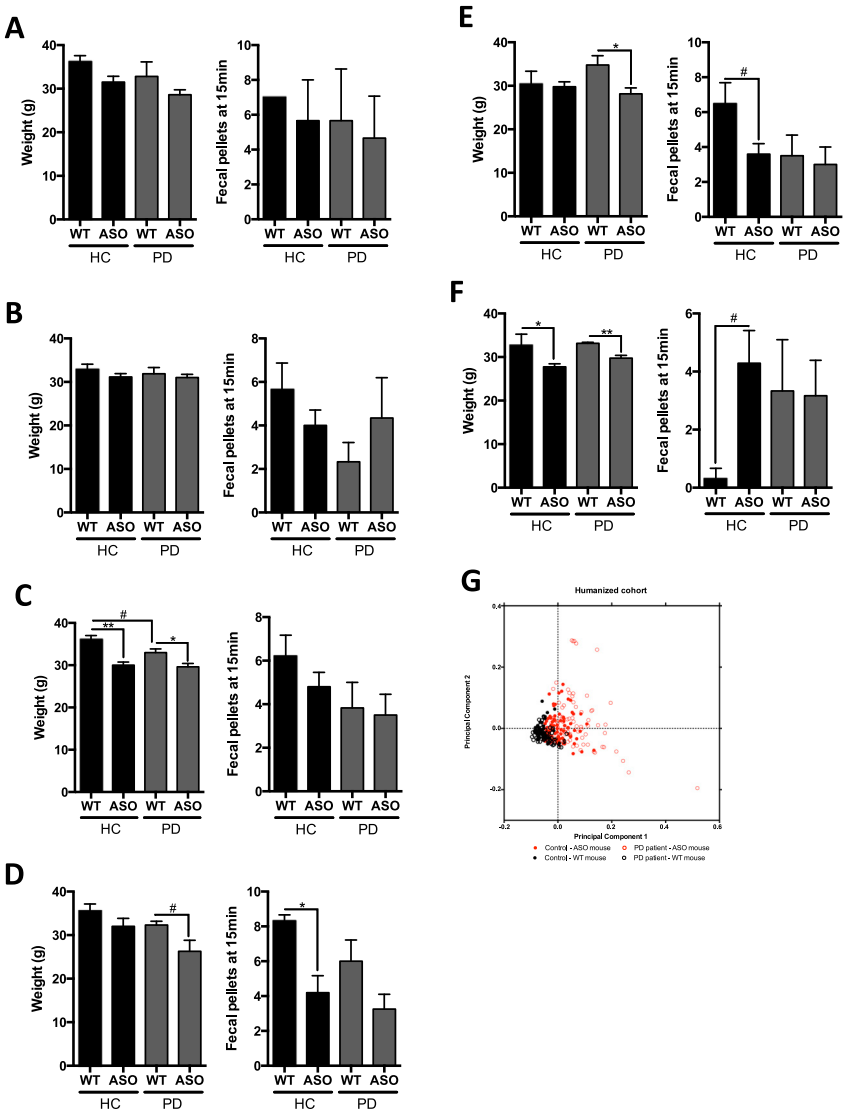

Figure S7. Body Weight and Fecal Output of Humanized Animals, Related to Figure 7

(A–F) Body weight and fecal output following 15 min in novel environment for each PD and HC humanized pair. (A) Pair #1, (B) Pair #2, (C) Pair #3, (D) Pair #4, (E) Pair #5, (F) Pair #6.

(G) Principle Component Analysis of compiled motor function between humanized animals.

Animals were tested at 12-13 weeks of age. N = 3-6, error bars represent the mean and standard error from 3 trials per animal. $^{\#}0.05 < p < 0.1$; $^{*}p \leq 0.05$; $^{**}p \leq 0.01$. HC = germ-free mice colonized with fecal microbes from healthy controls, PD = germ-free mice colonized with fecal microbes from Parkinson's disease patients, WT = wild-type, ASO = Thy1-α-synuclein genotype.